MULTIPLEXED END-POINT MICROFLUIDIC CHEMOTAXIS ASSAY USING CENTRIFUGAL ALIGNMENT

by

Sampath Ramaa Krishna Satti

B.Tech., Indian Institute of Technology Bombay, 2014

A THESIS SUBMITTED IN PARTIAL FULFILLMENT OF

THE REQUIREMENTS FOR THE DEGREE OF

MASTER OF APPLIED SCIENCE

in

THE FACULTY OF GRADUATE AND POSTDOCTORAL STUDIES

(Biomedical Engineering)

THE UNIVERSITY OF BRITISH COLUMBIA

(Vancouver)

November 2019

The following individuals certify that they have read, and recommend to the Faculty of Graduate and Postdoctoral Studies for acceptance, a thesis/dissertation entitled:

Multiplexed End-Point Microfluidic Chemotaxis Device With Centrifugal Alignment

submitted by Sampath Ramaa Krishna Satti in partial fulfillment of the requirements for

the degree of Master of Applied Science

in Biomedical Engineering

Examining Committee:

Hongshen Ma
Supervisor

Christian Kastrup
Supervisory Committee Member

Dana Grecov
Additional Examiner

Abstract

A fundamental challenge to the scalability of microfluidic chemotaxis assays is the requirement for time-lapse imaging to continuously track migrating cells. Current assays are not suitable for drug testing and drug screening applications that require the ability to perform hundreds of experiments in parallel. End-point chemotaxis assays wherein cells are aligned at fixed starting point before migration have been proposed as an alternative to continuous tracking. Previous methods developed to align cells use fluid flow to pattern cells in traps or constrictions, requiring external instrumentation and subjecting the cells to high shear stress. By patterning cells through centrifugation in our microfluidic device, alignment can be achieved without precise flow control while applying minimal shear stress to cells. This technique is insensitive to cell geometry and is capable of handling rare cells in the liquid sample. Additionally, as the chemical gradient in the assay is generated through passive diffusion, the stand-alone device can be placed in the incubator and subsequently imaged to obtain the migration characteristics in each of the 12 devices on our substrate. The device was used to observe the response of human neutrophils to gradients of fMLP. Our study reveals the potential to leverage cell alignment through centrifugation to develop highly scalable, end-point microfluidic chemotaxis assays.

Lay Summary

In this thesis, I have built such a physical device to analyze neutrophil cells. Neutrophils are one of the many types of white blood cells in the body. Neutrophils are recruited and gather to areas in the body with infection as well as damage. Distress signals that are released from infected are detected by neutrophils, which then migrate towards the source. This is part of the healing process. Neutrophils from a small amount of whole blood can be added this physical device, where they are aligned along a starting line. Their migration towards a chemical source can be captured using a single snapshot similar to a photo finish image at a 100 metres dash event. Development of a technology to analyze migration can therefore inform on the neutrophil health and how it is affected by various drugs.

Preface

All the research work reported in this thesis was designed, executed and analyzed by Sampath Satti and Hongshen Ma.

Assistance in cell culture and neutrophil-like cells were provided by Kerryn Matthews of the Multiscale Design Lab.

Human neutrophils for this study were obtained from healthy donors between the ages of 18 and 70 were included in this study, following informed consent and in accordance with University of British Columbia Research Ethics Board guidelines (UBC REB H10-01243)

Table of Contents

List of Tables

List of Figures

List of Equations

List of Abbreviations

BSA Bovine Serum Albumin

CD Compact Disc

CNC Computer Numerical Control

dHL60 Differentiated Human-Leukemia 60 cells

ECM Extracellular Matrix

FBS Fetal Bovine Serum

FEM Finite Element Modelling

fMLP N-formyl-methionyl-leucyl-phenylaniline

IL8 Interleukin 8

PEGDA Poly(ethylene glycol) Diacrylate

PDMS Poly Dimethyl Siloxane

Acknowledgements

To Hong, for all the brainstorming, troubleshooting, problem solving and guidance over the years.

To Drs. Kastrup and Grecov, for taking time out of their busy schedules to be on my examining committee and providing valuable feedback.

Folks past and present at the Multiscale Design Lab for training me, performing experiments together and being great company.

Folks I've met in Vancouver who I am extremely lucky to call friends, thank you for introducing me to new perspectives and well, just hanging in general.

To family in North America that has supported me through multiple surgeries and reminded me that home is close(ish). నాము౫ and తాతాయి, your blessings got me here. To అమ్మా, నాన్నా and Chandan, you have and will remain my strongest supports. Thank you all for coming on this roller-coaster with me.

It would be entirely factual to say that my blood, sweat and tears went into this thesis.

Chapter 1: Introduction

In this section, the phenomenon of chemotaxis is introduced. Specifically, the response of human neutrophils to chemoattractant molecules is discussed in detail. Later, examples of various in vitro assays used to produce clinically relevant information relevant to human health and disease states is presented.

1.1 Cell migration and chemotaxis

Cell migration is a fundamental process in the biological world. At the single cell level, cell migration is useful to the organism in search of food as well as mating[1]. E coli bacteria migrate towards sources of food such as sugar[2]. Cell migration performs more specialized roles in multicellular organisms, functioning to mediate organization, embryogenesis and maintain homeostasis. Cell migration is regulated by various membrane receptors, cellular pathways and actuated by the actin cytoskeleton.

Chemotaxis is a subset of cell migration where there is a directed migration of cells in response to a chemical gradient. It is characterized by the following features that distinguish chemotaxis from other migratory behaviors such as Haptotaxis and Electrotaxis as well as random movement

Soluble fluid phase chemical gradient

Chemotaxis is the ability to migrate towards a source of chemical gradients. In particular, the gradient must be present in the fluid phase for the migration to be termed chemotaxis. In the case of chemical molecules either being expressed on or bound to a surface in a gradient, the observed

response is termed Haptotaxis[3]. Directed cell response in response to an electrical signal is called Electrotaxis.

Taxis versus kinesis

Taxis refers to the general movement of an organism in response to a stimulus. These innate behavioral responses can occur as a response to various stimuli. A taxis is characterized by organism motility as well as guided movement in response to the stimulus[4]. A kinesis is a simpler change in overall activity without any directional component. Chemotaxis is characterized by a clear directional motility towards the chemical gradient. Chemokinesis however, is simply an increase in cell motility and activity that is not directionally biased.

1.2 Clinical relevance of neutrophil chemotaxis assays

Chemotaxis is an important aspect of many biological processes and diseases, such as the immune response to infection[5], wound healing[6], inflammation[7], embryogenesis[8] as well as cancer metastasis[9].

Neutrophils are circulating cells in the human body and are part of the innate immune system response. They are normally found in the blood stream and have the ability to phagocytose (ingest) other particles, foreign bodies or dying cells. Neutrophils are the first responders as a part of the inflammatory response. Neutrophils have the ability to migrate and reach the source of the infection through chemotaxis. Therefore, neutrophil chemotaxis is intimately linked to many biological process and disease states.

In a review of the available literature in the field[10], Zonneveld et al found that automated analysis of neutrophils at the bedside led to better treatment protocols and patient outcomes. Of the many features of neutrophils that can be analyzed, their migratory potential was assigned special importance in the context of septic shock. Since the chemotactic response of neutrophils in patients with septic shock is lower that healthy controls, the assay can be used as a marker for the disease state. In a scenario like asthma, neutrophils are highly activated and have higher migratory potential, as demonstrated by Sackmann et al[11].

Butler et al established the decreased directional migration velocity of neutrophils in patients with burn injuries using a microfluidic chemotaxis assay[12]. Averaged neutrophil migration velocities in patients with burn injuries were compared to a baseline established using samples from healthy volunteers. The study found decreased neutrophil migration velocities as early as 24 hours after the injury, bottoming out at the 72-hour mark and improving thereafter. This study demonstrated the efficacy and suitability of chemotaxis assays as a strong indicator of disease progression.

Berthier et al have also established the utility of chemotaxis assays in the context of diagnostics and characterization of rare diseases[13]. On presentation with recurring bacterial infections, a patient was diagnosed with an immunodeficiency disorder. Running the neutrophils from the patient sample through the chemotaxis assay demonstrated a lack of neutrophil polarization as well as impaired motility. Later, a Rac2 mutation that is known to impair leukocyte morphology

as well as migration was discovered in the patient validating the observations made through the chemotaxis assay.

Chemotaxis therefore has a high degree of biological and clinical relevance, and chemotaxis assays have great utility in various applications. Figure 1.1, shows a few promising applications for chemotaxis assays. With the increasing focus on using microfluidics devices for point of care diagnostics, developing organ-on-chip devices for drug testing as an alternative to animal models and integrated -omics platforms, chemotaxis assays and migratory platforms will be an important component going forward.

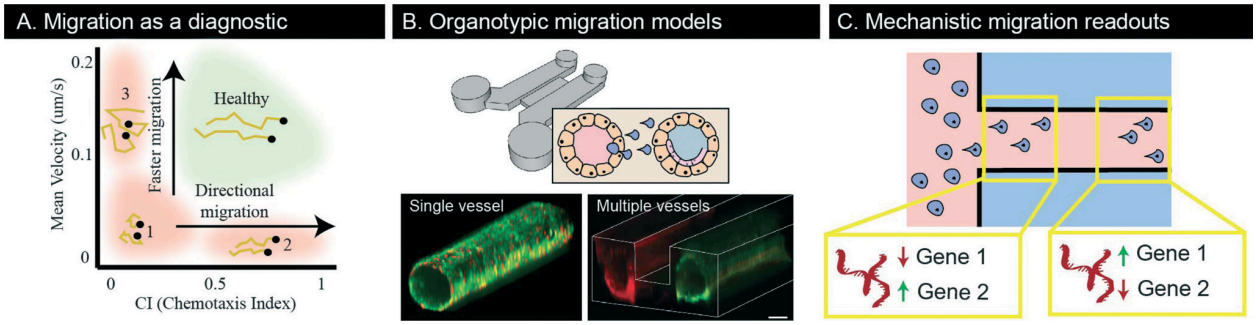

Figure 1.1 Various applications of chemotaxis assays including their use for diagnostics, mechanistic readouts and studying migratory behavior in vitro[10]. Reproduced with permission.

1.3 Biology of neutrophil chemotaxis

Chemotaxis, specifically in neutrophils, can be modelled and understood through a framework wherein a stimulus sensed by the cell is processed through the internal chemical pathways resulting in an observable change in activity and morphology.

Input – Molecules binding to cell receptors (or cell-cell receptor binding in case of collective migration) provides a stimulus to the cell either in the temporal or the spatial domain (Figure 1.1). Common molecules that induce a chemotactic response in neutrophils include Interleukin-8 (IL8, also known as CXCL8) as well as a bacterially synthesized peptide, N-formyl-methionyl-leucyl-phenylaniline (fMLP)[14].

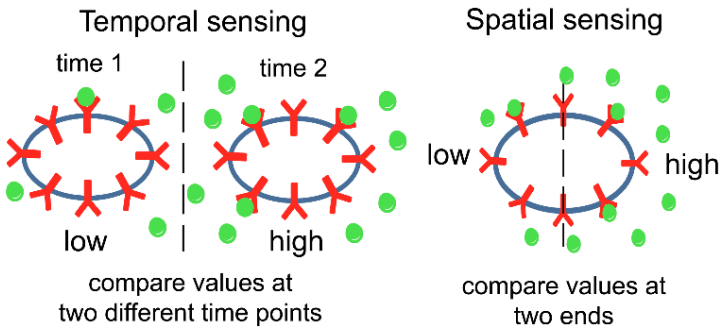

Figure 1.2 Spatial and temporal chemical sensing paradigms to explain chemoattractant binding to cell receptors[15]. Reproduced with permission

IL-8 is released by macrophages as part of the innate immune response in the human body and binds to CXCR 1/2 receptors on the neutrophil surface. This stimulates the neutrophils to upregulate integrin expression, facilitating cell adhesion with extracellular membrane ligands such as fibronectin or collagen. This cell adhesion process is crucial to the polarization and reorganization of the actin filaments that form the cytoskeleton, thereby causing a migratory response[16].

While IL-8 is an endogenous chemoattractant signaling inflammation, neutrophils are also capable of responding to exogenous chemoattractants such as fMLP. fMLP have bacterial or mitochondrial origins and are found in higher concentrations at sites of bacterial infection or trauma[17].As part of the neutrophil's role in the innate immune system, the cells have receptors (G Couple Protein receptors, GPCR) capable of binding to fMLP. This causes receptor phosphorylation and downstream upregulation of the factors responsible for directed migration towards fMLP.

Computation – Chemical pathways within the cell that are activated on receptor binding and causing downstream signaling effects such as cell actuation. In neutrophils, once chemoattractants such as fMLP bind to receptors (GCPR), it sets off a downstream signalling cascade within the cell involving various proteins and kinases such as PI3K and p38 MAPK[18].

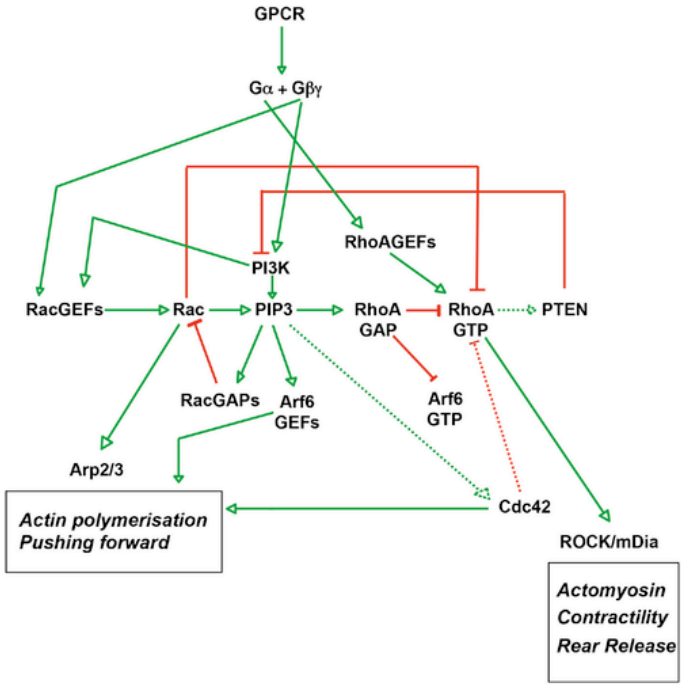

Figure 1.3 Chemical pathways in neutrophils that regulate chemotaxis[18]. Reproduced with permission.

Output – Mechanical actuation of the cell is achieved through Actin polymerization and reorganization. The Arp 2/3 complex (Figure 1.3) that is produced as a result of the receptor binding causes the production of actin filaments from monomer units. These actin filaments produce a leading-edge protrusion in the neutrophil causing polarization and cell locomotion. At the same time, contractile forces are generated at the back to release the cell from the substrate at those locations.

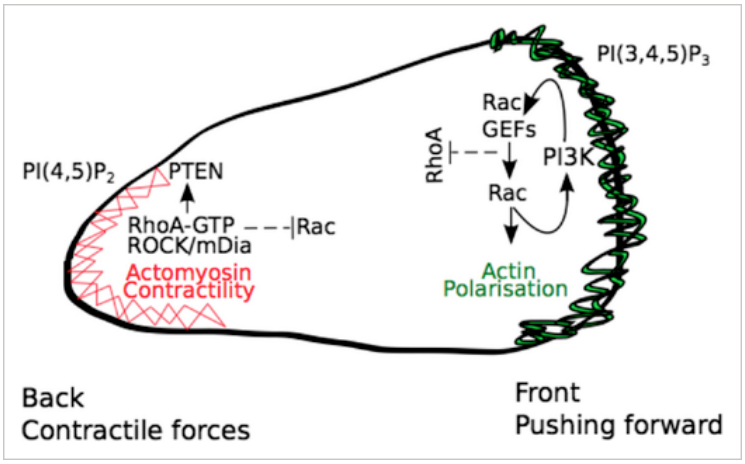

Figure 1.4 Various biological processes responsible for cell actuation[18]. Reproduced with permission.

1.3.1 Practical considerations for neutrophil chemotaxis assays

Both fMLP and IL8 induce a strong chemoattractant response in neutrophils in vitro, increasing the directedness of the chemotaxis response, as well as migration velocity[19]. As noted previously, the extracellular matrix has a large role to play in the migration and is therefore an important factor to consider while developing chemotaxis assays.

Access to neutrophils for experiments is only though isolation of the cell type from whole blood. The isolation can be either done through density separation or immunomagnetic separation. However, once neutrophils have been extracted from whole blood, they must be used for chemotaxis experiments within 4-8 hours[20]. Therefore, the availability of an immortal human leukemia cell line (HL-60) that can be differentiated to granulocytes at any stage, provides a viable and attractive alternative to neutrophils for biological experiments.

Chapter 2: In vitro Chemotaxis assays

This chapter looks at the various in vitro assays developed to observer and measure the response of cells to chemical gradients. Section 2.1 looks at the traditional chemotaxis assays developed before the advent of microfluidics. The section concludes with a comparison of different traditional assays, highlighting their advantages as well as disadvantages. Section 2.2 provides a brief introduction to the field of microfluidics and briefly covers the physics governing fluid flow. Later, various techniques and device topologies used to generate chemical gradients in microfluidic devices are presented. A sample of microfluidic chemotaxis assays are presented and compared in section 2.2.3. Section 2.3 identifies the limitations of current microfluidic chemotaxis assays and introduces the concept of an end-point chemotaxis assay. With this context, Section 2.4 talks about the various cell alignment methods in microfluidic devices and compares their advantages and disadvantages .

2.1 Traditional chemotaxis assays

This section will briefly look at various traditional chemotaxis assays such as the Transwell, 2D chamber assay and the micropipette assay. It will also identify their advantages as well as shortcomings and present the results in Table 2.1. A simplified schematic of the working of each chemotaxis assay is presented in Figure 2.1. Each assay will be discussed in detail subsequently.

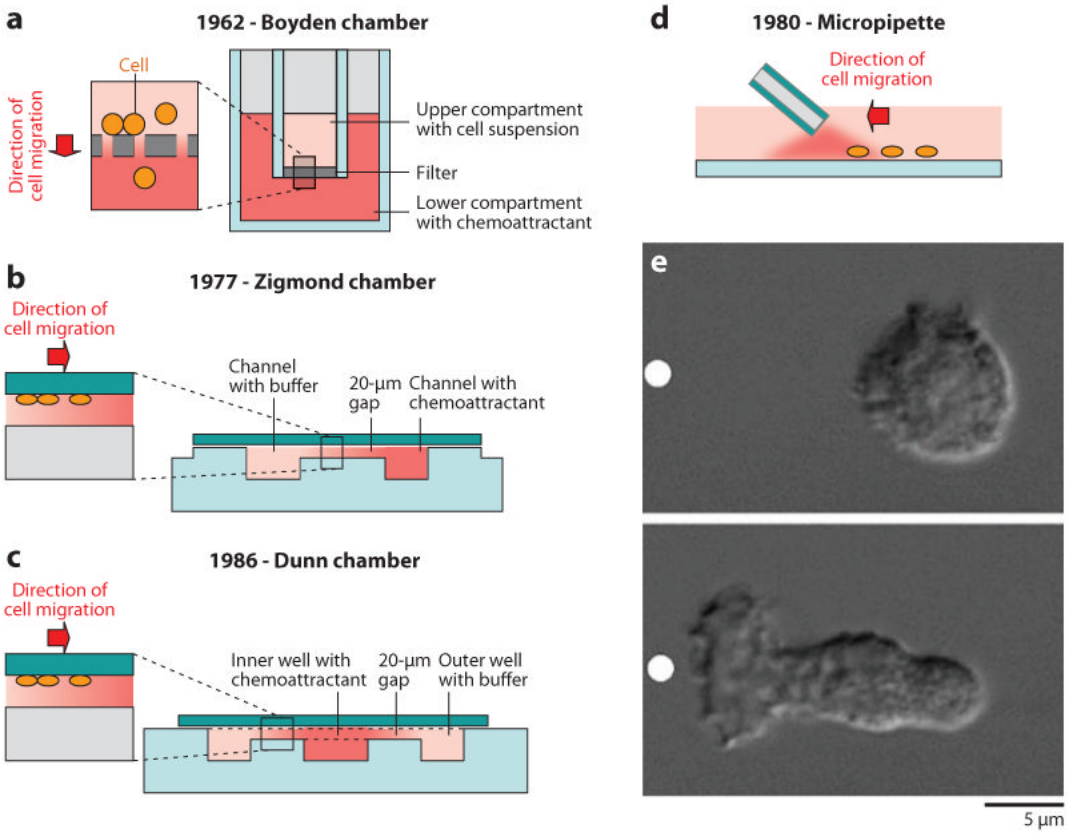

Figure 2.1 Schematics of traditional chemotaxis assays[21]. Reproduced with permission.

2.1.1 Transwell assay

Developed in 1962, the Transwell or the Boyden assay remains one of the most popular in vitro chemotaxis assays to this day. The assay consists of a chamber with a porous membrane (similar to a basket) that divides a microwell into two sections when inserted in the latter[22]. This configuration can be seen in Figure 2.1a. Cells are added to the chamber on top of the porous membrane while the chemoattractant is added to the lower chamber (below the membrane). The diameter of the pores in the membrane can be chosen depending on the size of the cells. Cells sense the chemical gradient established across membrane and migrate into the lower chamber

through the pores. At the assay endpoint, the cells in the bottom chamber are counted. The fraction of the cells that migrate is indicative of the chemotactic potential.

The Transwell assay is readily amenable for scaling owing to its simplicity and compatibility with traditional micro well plates. Robotic handlers and automated analysis equipment designed for imaging well plates can be readily adapted to run the Transwell assay in a high throughput setting. However, the assay has many drawbacks. The readout at an individual cell level is only binary. The assay only captures information as to whether the cell has made it across the membrane or not. More complex behaviors cannot be observed using this assay. Additionally, the chemical gradient at the micropore interface varies with time and cannot be quantified.

2.1.2 2D chamber assays - Zigmond, Dunn, Soon

The Zigmond[23], Dunn[24] and Soon chambers are all various implementations of a similar principle of achieving a 2D chemotaxis assay. Briefly, two wells engraved into a glass substrate are connected by a thinner bridge channel. Chemoattractant solution is added into one well, while buffer along with cells are added into the other well. A cover slip is placed on top of this device, which connects the fluid in the wells through the bridge channel. This results in diffusion of the chemoattractant from one well to the other in a slow and controlled manner. The cells are observed under a microscope in the bridge channel.

Wells in a Zigmond chamber are parallel to each other, while those in a Soon chamber are organized radially. The buffer well in a Dunn chamber is rectangular and is surrounded by the chemoattractant well. While 2D chemotaxis assays provide for a more detailed analysis and cell

tracking, the fabrication processes used result in experiments with a high degree of variability and non-uniform gradients. The assay cannot be scaled in order to perform multiple chemotaxis experiments in parallel.

2.1.3 Micropipette assay

Developed in 1980, the micropipette assay generates a gradient through constant perfusion of chemoattractant solution into a well of much greater volume[25]. The chemoattractant concentration, which is highest at the outlet of the micropipette, decays exponentially as it spreads creating a gradient in the vicinity. Placing the micropipette near a desired cell can elicit a response at the single cell level which can be visualized through optical microscopy.

The technique is capable of capturing single cell response and behavior, useful for understanding the cell dynamics and pathways leading to cytoskeleton polymerization and reorganization. However, the technique cannot be scaled up for a population of cells as is usually the case. Additionally, the gradient cannot be quantified and depends on various parameters such as flow rate, pipette tip diameter, position within the well and orientation. It also requires the use of a large amount of chemoattract solution which can be quite expensive. The assay is also not suitable for longer assay durations as the continuous perfusion of chemoattractant solution into the reservoir can saturate the solution and weaken the chemotaxis response.

	Notes	Advantages	Disadvantages
In Vitro Methods	- Various chemotaxis assays regularly used in benchtop experiments	- Control over experiment and ability to tune parameters - Suitable for drug testing, screening and diagnostics	- Traditional invitro methods do not capture the complexity and nuance of conditions in vivo and hence do not measure true migratory response
Transwell Assay	- Cells undergo migrate through a micropore membrane subject to a chemical gradient	- Easy integration with microwell plates - Simple readout, can be made high throughput	- Output of assay at the cellular level is binary (low information)
2D assays (Zigmond, Dunn, Insall)	- 2D Migration of cells on a surface is observed in the presence of a gradient	- Cell migration paths can be observed yielding metrics of higher quality	- Established gradient is non-uniform, unstable and not quantitative - Variability in experiment
Micropipette Assay	- Continuous perfusion of chemoattractant into well to produce a local gradient -Cells move to source of chemoattractant	-Good control over spatio-temporal chemical stimulus -Useful to understand cell processes leading to chemotaxis and locomotion	- Gradient cannot be quantified and is extremely variable - Chemotaxis of only few cells in the the vicinity can be observed

Table 2.1 Comparison of various traditional chemotaxis assays and paradigms

2.2 Microfluidic chemotaxis assays

With heterogeneity among cell populations having increased clinical relevance[26], as well as the desire to obtain data at a single cell resolution while increasing experiment throughput[27], the shortcomings of traditional chemotaxis assays were increasing evident. This resulted in a need for a new generation of chemotaxis assays capable of generating quantifiable, robust chemical gradients to replicate in-vivo microenvironments being studied as well as the ability to run multiple independent experiments with in parallel. Achieving these goals requires a paradigm shift in the design, fabrication and analysis of these assays, which was achieved through the use of microfluidic technologies and devices.

2.2.1 Introduction to microfluidics

Microfluidics is the science of fluid physics and manipulation at the microscale level. In microfluidic devices, fluids are constrained to flow in channels with dimensions in the micrometer scale. The origins of microfluidics can be traced back to the microfabrication tools developed for silicon transistors as well as Microelectromechanical Systems (MEMS)[28]. Combined with the need for rapid analytical measurements of small analytes in the field of biology and chemistry, the field of microfluidics has had a rapid rise.

The applications of microfluidics span across the domains of diagnostics and personalized medicine, chemical synthesis, organ printing as well as new frontiers such as renewable energy. The inkjet printer nozzle head is an example of a commercially successful microfluidic technology[29]. Microfluidic technology was perfectly suited for the need to achieve uniform femtoliter sized droplet generation and dispensing on demand.

2.2.2 Centrifugal microfluidics

Centrifugal or CD microfluidics is one implementation of microfluidic systems that offers holistic micro Total Analysis (uTAS) by arranging microfluidic networks around a circular disc in radial fashion. This disc is rotated about its central axis to accomplish various functions. Such a system is capable of generating pressure gradient to establish fluid flow, valving functions, mixing, separation and analysis[32] [33]. The arrangement of the devices on the disc also enables running parallel experiments under various conditions. While a few examples of centrifugal microfluidic devices are presented in later sections, a brief overview of the physics at play in these devices is offered here.

Non-inertial frames of reference A rotating disc is considered to be a non-inertial frame of reference which supersedes the analysis of forces acting on fluids and particles on such a disc. These pseudo forces include the centrifugal force (F_ω), the Coriolis force (F_{co}), and the Euler force (F_e) and are shown in Figure 2.2

Equation 2.1 Centrifugal Force

$$F_\omega = -m\omega \times (\omega \times r)$$

Equation 2.2 Coriolis Force

$$F_c = -2m\omega \times \left(\frac{dr}{dt}\right)$$

Equation 2.3 Euler Force

$$F_e = -m\frac{d\omega}{dt} \times (r)$$

Where, m is mass, ω is the angular speed of rotation while r is distance from the axis of rotation.

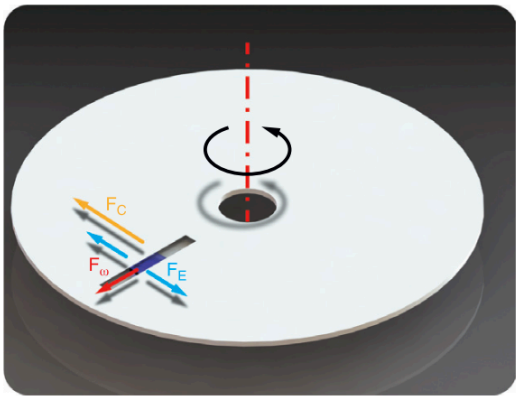

Figure 2.2 Forces in a rotating centrifugal microfluidics system[33]. Reproduced with permission.

The centrifugal force is the most commonly observed force in such systems, especially under steady state when $\frac{dr}{dt}$ and $\frac{d\omega}{dt}$ are both zero. In the rotating frame, the centrifugal force is exerted radially outwards on any fluid particle in a channel. The Coriolis force is perpendicular to the centrifugal force and is only observed under transient conditions when a particle is moving along the radial direction. The Euler force is only observed during any change of the rotation speed of the assembly (such as the start/stop).

Additionally, for a given fluid column of density ρ of between inner radial point r_1 and outer radial point $r_2$being rotated at an angular velocity of ω, the pressure differential on the column due to the centrifugal force can be calculated to be

Equation 2.4 Pressure difference due to centrifugal forces

$$\Delta P_\omega = \frac{1}{2}\rho\omega^2({r_2}^2 - {r_1}^2)$$

For particles transport inside fluids such cells suspended in liquids, there is a net force on the particle relative to the fluid given by

Equation 2.5 Drag force due to centrifugal forces

$$F_{relative} = \frac{1}{2}A(\rho_{particle} - \rho_{fluid})\omega^2 r^2$$

Where, A is the particle cross section, $\rho_{particle}$ is the density of the particle and ρ_{fluid} the density of the fluid. This relative force is responsible for causing particle sedimentation and centrifugation in these devices.

2.2.3 Gradients in microfluidic devices

The ability to control fluid in a deterministic fashion, including processes such as mixing, and diffusion are key to achieving robust, quantitative chemical gradients of chemoattractants for assays. Microfluidic technologies equip researchers with the tools to create such gradients. In this section, a few different ways in which gradients can be generated in microfluidic devices will be compared.

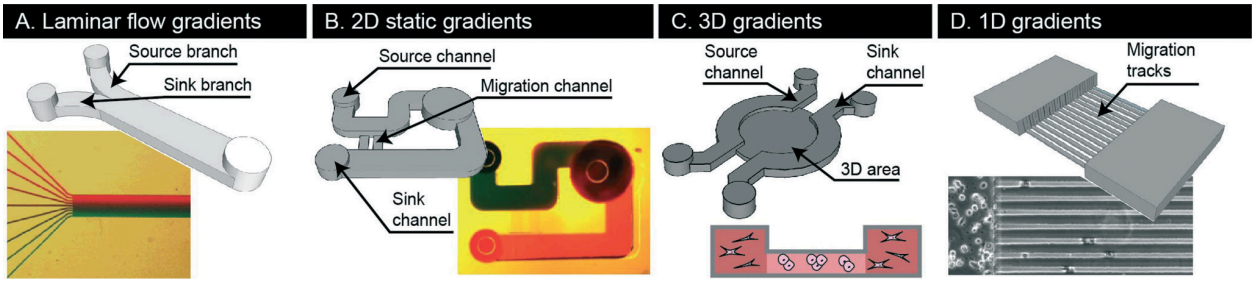

Figure 2.3 Microfluidic gradient generation methods[21]. Reproduced with permission.

2.2.3.1 Laminar flow gradients

Laminar flow gradients are created in a simple T-shaped microfluidic geometry where two branches of fluid are merged into a larger channel. In the scenario where the branches contain a different concentration of chemoattractant, the diffusion across the fluid streamlines in the merged channel creates a chemical gradient. To achieve linear gradients, multiple branches with more steps in concentration can also be merged as seen in Figure 2.2 (Panel A, inset). Leveraging the principles of laminar flow, any number of input branches with different concentrations can be created by repeatedly splitting, merging and mixing two input source and sink branches. This method of achieving linear gradients is also colloquially called the "Christmas tree design" due to the visual shape of the microfluidic network that results.

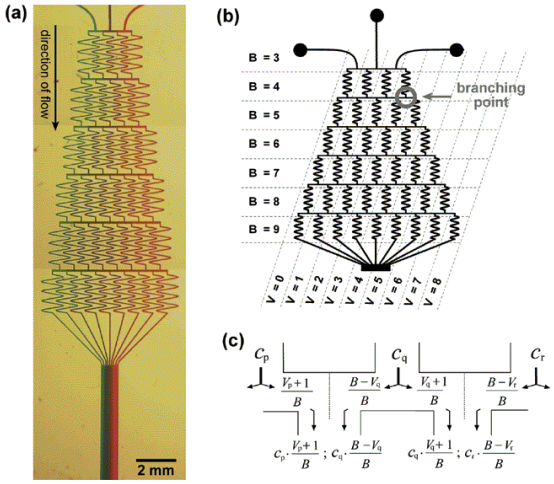

Figure 2.4 Microfluidic network for generating complex gradients[34]. The gradient is generated through repeated dilution of a fluid stream to produce intermediate concentrations. These are subsequently merged into a larger channel where a steady state gradient is generated. Reproduced with permission.

2.2.3.2 2D static gradients

Statics gradients are a simple, passive way to generate chemical gradients without the need for external syringe pumps or pressures sources. 2D static gradients have been used to create gradients in the traditional Zigmond and Dunn chambers assays. These gradients however suffered from a lack or gradient repeatability and accuracy. Microfluidics technology can alleviate these problems to generate stable, consistent gradients.

Diffusion is an important phenomenon that is key to generating passive gradients. In one dimension, the net distance moved by a particle due to diffusion is governed by diffusivity and time according to the following formula

Equation 2.6 Diffusion length

$$d^2 = 2Dt$$

where d is the migration distance due to diffusion, D is the diffusion constant and t, the time of diffusion. From this relationship, it is evident that length scales play an important factor in the effect diffusion has. In most 2D passive gradients, source and sink reservoirs abut the gradient channel on either end. The source reservoir is filled with the chemoattractant solution, which slowly diffuses into the gradient channel. Since the volume of the reservoirs is designed to be many orders ($O(3)$) larger than the gradient channel, which also has a high resistance designed to limit chemical flux, the concentration of the reservoirs can be assumed to be constant over the duration of the experiment (many hours). This fixed concentration at either ends of the gradient channel results in a steady state condition. Over extended periods of time, flux transport from the source to the sink reservoir will equalize the concentration leading to a loss of the gradient.

Any fluid flow in a channel with a passively generated gradient can disturb the gradient and interfere with any chemotactic movement desired to be observed. As a result, various strategies have been proposed to either eliminate the causes or work around their effects. In most scenarios, unequal evaporation from the reservoirs is responsible for causing flow in the gradient channel. This can be eliminated by saturating the experiment environment to 100% Relative Humidity or covering the inlet to the reservoirs with Petroleum Jelly or Mineral Oil. In situations when elimination of flow is not possible, solutions to mitigate the effect have been proposed. A parallel bypass channel can be used to divert the bulk of the flow. This solution can be conceptually explained through the electronic-hydraulic analogy, wherein source and sink reservoirs are voltage potential nodes and the migration and bypass channels are fluidic resistances between the two nodes. The ratio of flow in either channel is in inverse ratio of their fluidic resistances. Connecting a low resistance bypass channel across a higher resistance migration channel results in the bulk of the current (fluid flow) going through the former (Figure 2.5)

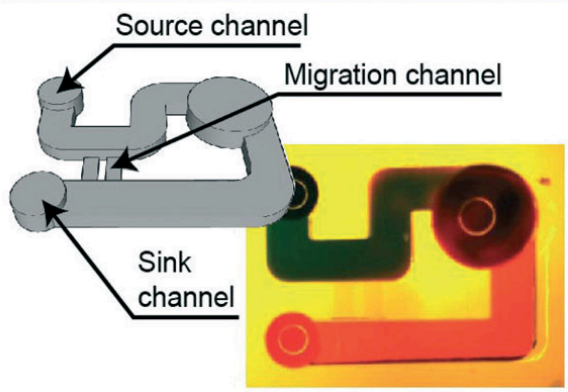

Figure 2.5 Bypass channel to reduce the effect of flow on concentration profile in a passive diffusion gradient device[13]. Adapted with permission.

2.2.3.3 1D gradients

1D gradients or perfused source sink (ladder) networks combine features of both active laminar gradients and passive source sink gradient networks. In these devices, while gradient channels connect the source and sink reservoirs in a manner resembling passive source sink gradients, fluid in the reservoirs is constantly perfused to keep the concentration at the sink and the source constant. Flow arising due to this perfusion does not affect the cells as it is only restricted to the source and sink channels while the cells being observed are located in the gradient channel. While this method requires the use of a larger volume of chemoattractant solution, it can also sustain gradients for as long as desired. Such long-term gradients are necessary to the design of microfluidic chemotaxis assays with tumour cells where the migration response is observed over multiple days. These networks are also called "ladder networks" owing to their visual similarity.

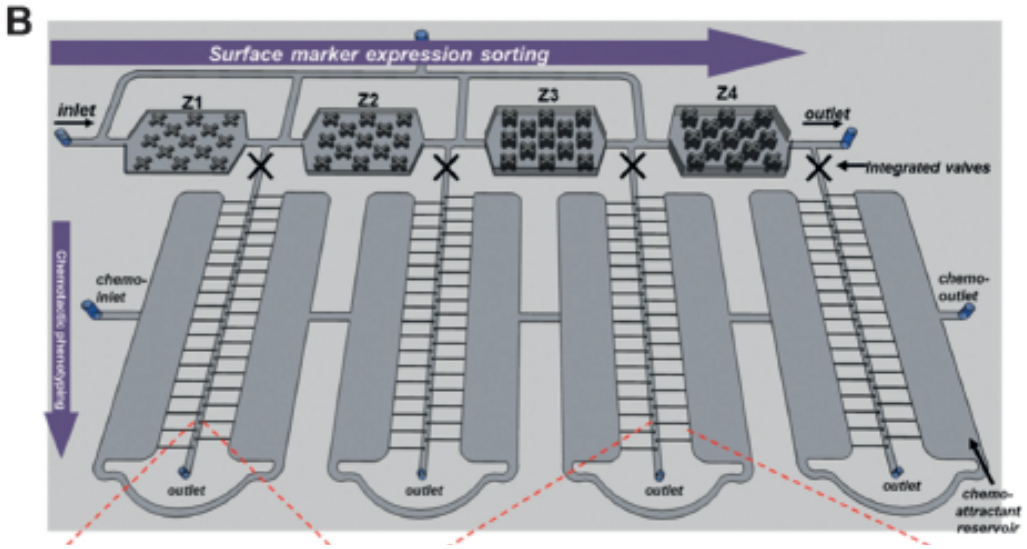

Figure 2.6 Perfused source sink gradient design[35]. The chemoattractant reservoir is constantly perfused to maintain the source concentration. Reproduced with permission.

2.2.4 Microfluidic chemotaxis assays

A broad selection of microfluidic chemotaxis assays reported in literature will be reported in this section. A few representative chemotaxis assays have been chosen so as to showcase the widest range of gradient generation and cell alignment techniques and important features of the assay subsequently compared.

2.2.4.1 Neutrophil chemotaxis to linear and complex gradients of IL8

Neutrophil chemotaxis to complex, quantifiable gradients of IL8 was measured in one of the first microfluidic devices used to study chemotaxis[36]. The device used a microfluidic device where an active gradient was generated through laminar flow. The major focus of this device lay on ensuring accurate, quantifiable gradient conditions in which cell migration could be quantified These neutrophils isolated from whole blood were added to the PDMS device where a gradient of IL8 was established through active laminar flow-based diffusion techniques. Neutrophils were found to migrate across the channel towards higher concentrations of IL8. Additionally, more complex gradients of IL8 were created such as valleys, hills and sawtooth curves.

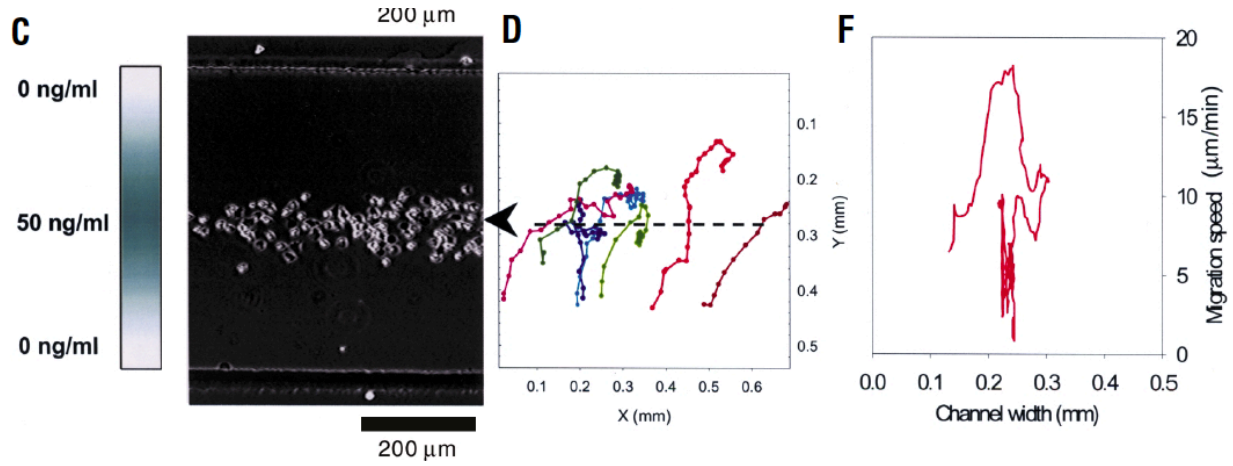

Figure 2.7 Neutrophils migrating in response to an IL8 'valley' within the microfluidic device[36]. Reproduced with permission.

2.2.4.2 Arrayed high-content chemotaxis assay

Once the viability of microfluidic devices to run chemotaxis assays was proven, the focus shifted to the applications of chemotaxis such as patient diagnosis and screening. In this work by Berthier et al, a high-throughput chemotaxis assay was developed that enabled the running of up to 50 separate experimental conditions in parallel[13]. These experimental conditions could vary in surface treatment, chemoattractant type as well as concentration. The gradient was generated using a passive source sink topology, where any residual flow was eliminated using a humidified chamber as well as a bypass channel. Prior to the addition of neutrophils to the device, it was treated with ECM proteins such as collagen, fibronectin, fibrinogen or laminin and BSA blocked later. Individual devices were arrayed on the platform in a way that it was possible to integrate with a robotic fluid handler. Additionally, device loading was done through the passive pumping technique, eliminating the need for extensive fluid pumps and tubing. The assay also alludes to end point analysis, by ensuring that no cells enter the gradient channel during the loading process. While it can be assumed that any cell migrating under the influence of the chemical

gradient starts at the edge of the gradient channel, it does not ensure that all the cells start migrating at the same time point.

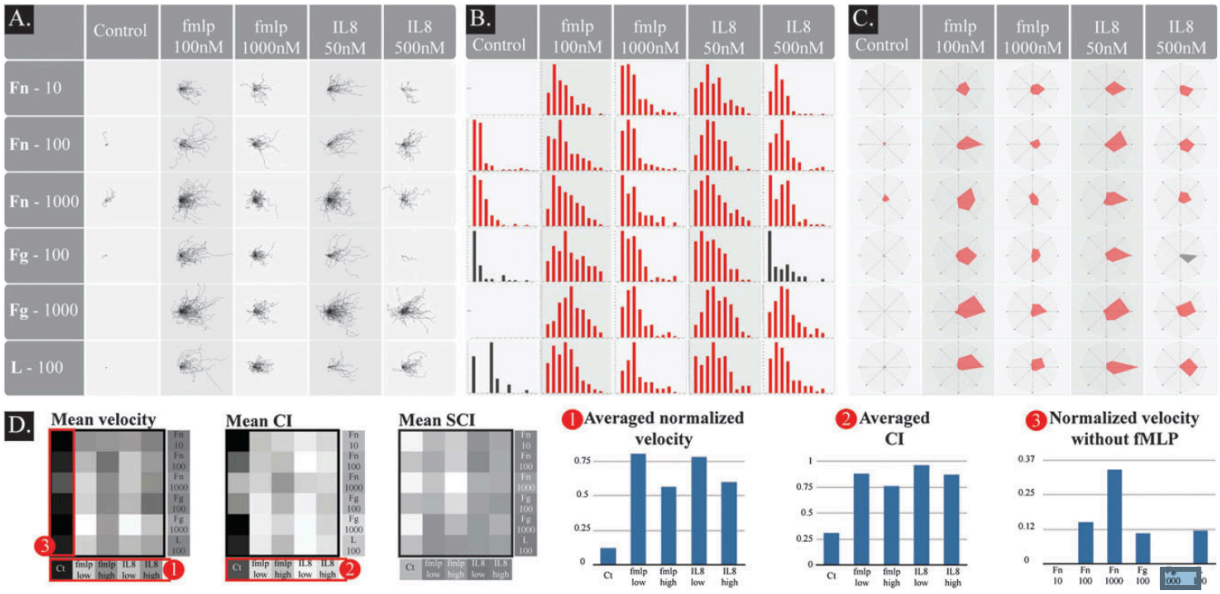

Figure 2.8 Screening human neutrophil migration on various ECM surfaces in response to fMLP and IL8[13]. Reproduced with permission.

2.2.4.3 Chemotaxis-based microfluidic selection

In this work, Chen et al develop the only microfluidic chemotaxis assay (known so far) able to stratify a population sample based on chemotactic potential [37]. Development of this functionality is a fundamental requirement to ensuring that chemotaxis platforms can be integrated with downstream omics analysis. The authors use a perfused source sink (ladder like) design (Figure 2.9), where the source channel includes serpentine channels to trap cells in designated spots to ensure uniform migration conditions for each cell. Once the cells migrate through the rails of the ladder network, into the source channel (Figure 2.9B), a solution containing trypsin is added to detach migrated cells and collect them (Figure 2.9C). Cells so collected were found to proliferate at higher rate in cultures as well as form larger sized colonies as compared to non-migrated cells.

One of the shortcomings of this device is limit of the scaling of the serpentine cell alignment technique as well as the binary nature of the cell separation.

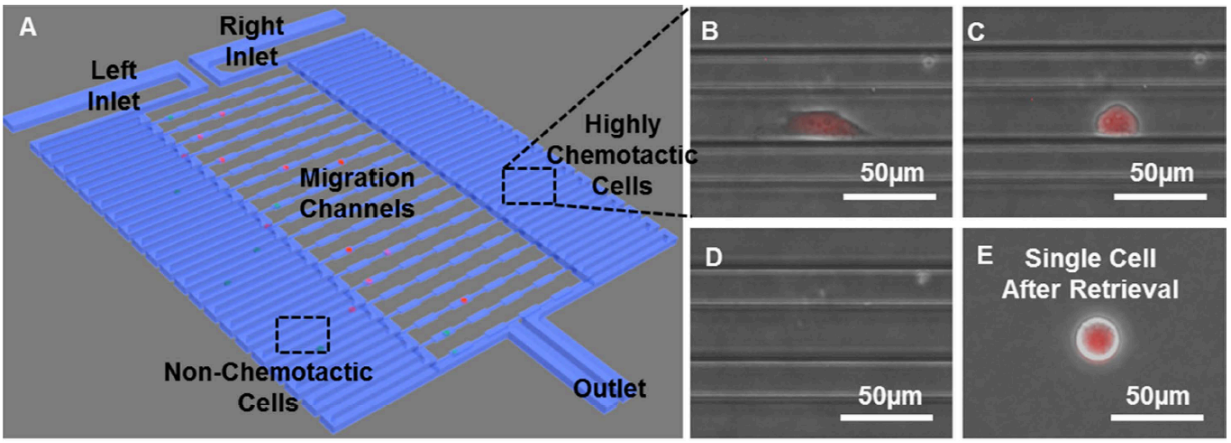

Figure 2.9 Cell separation using chemotaxis[37]. Trypsin is flowed through the right channel to collect the cells that have migrated across at the outlet. Reproduced with permission.

2.2.4.4 Dual-docking microfluidic chemotaxis assay

In this work, a compact passive perfused source sink device is developed as a standalone chemotaxis assay for patient diagnosis[38]. Constant perfusion of the source/sink channels is achieved by loading the loading the source/sink reservoirs with fluid (and periodically aspirating media from the outlet). This results in a gravitation potential driven flow that can be sustained for up to 6 hours. A cross flow is also set up to dock/align the neutrophils at one end of the gradient channel though the design of a constriction (Figure 2.10 C). The readout of the device is established through optical microscopy.

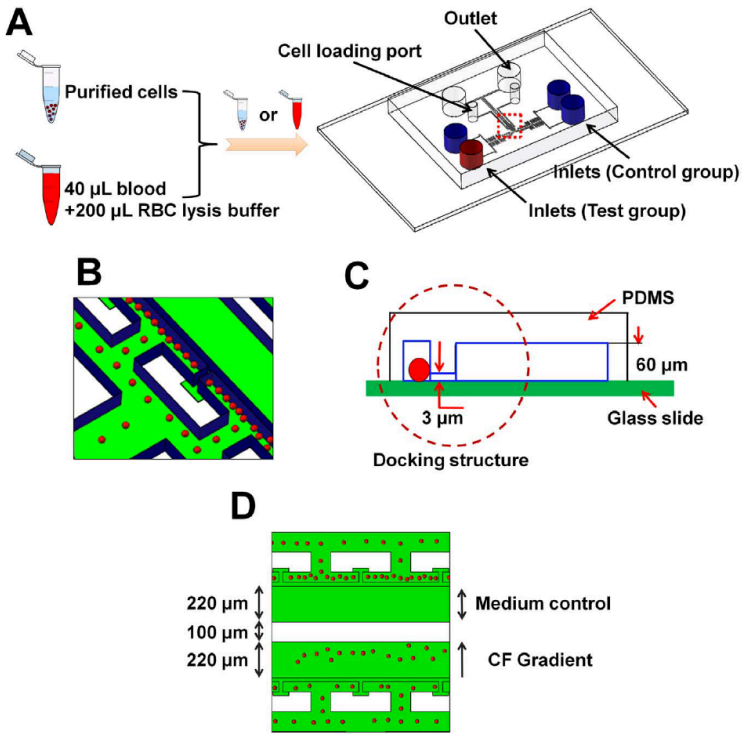

Figure 2.10 Docking device to align neutrophils from whole blood prior to migration[39]. The cell loading port is filled in such a way to ensure a higher pressure on the cell inlet to be able to dock cells. Reproduced with permission.

	Cell Type used	Gradient Method	Chemo-attractant	Concentration Strengths	Cell speeds / velocities	High Throughput?	Cell Alignment?
Jeon, 2002 [36]	Human Neutrophils	Active Laminar flow	IL8	50ng/ml over 500um	N/A	No	No
Berthier, 2010 [13]	Neutrophils Human+ dHL60	Passive Source Sink	fMLP, IL8	0-1000nM (fMLP), 0 - 500nm (IL8)	0.14 um/s (100nM fMLP)	Yes	No Alignment but end-point analysis possible
Boneschansker, 2014 [40]	Human Neutrophils	Perfused Source Sink Channels	fMLP	100nM over 800um	20um/min (in 6um channels)	No	Yes (DiCarlo traps)
Sackmann, 2012 [41]	Human Neutrophils	Passive Hydrogel source	fMLP	100nM over 2000um	**Speed** 6um/min (2D) **Dir. Velocity** 1.5um/min	Yes	No
Yang, 2017 [38]	Human Neutrophils	Perfused Source Sink channels (passive)	fMLP	100nM over 300um	0.2 um/second	No	Yes

	Cell Type used	Gradient Method	Chemo-attractant	Concentration Strengths	Cell speeds / velocities	High Throughput?	Cell Alignment?
Poudineh, 2017	LnCAP, PC3, PC3M	Perfused source/sink channels	CXCL-16	100ng/ml over 1000um	25um/hour	No	Yes (serpentine)
Chen, 2015	SKOV3	Perfused source/sink channels	HGF	50ng/ml over 1000um	~15um/hour	No	Yes

Table 2.2 Comparison of various microfluidic chemotaxis assays and devices showing the nature and source of chemical gradients as well as a brief overview of obtained results.

2.3 Limitations of existing microfluidics chemotaxis assays

While microfluidics technology has addressed some of the shortcomings of the aforementioned traditional chemotaxis assays and opened up further avenues of inquiry, there are still a few gaps that need to be addressed. This gap is further evinced by the lack of microfluidic chemotaxis devices that have achieved ubiquity on the same scale as pulse-oximeters at the patient bedside or hematology analyzers in laboratories.

This can be attributed to the following limitations of most microfluidic chemotaxis assays

1. **Need for real time continuous tracking** – Cells currently need to be tracked continuously under a microscope and later analyzed to extract the relevant metrics. Using automated microscope stages, researchers are capable of running multiple experiments in parallel by cycling through each observation location. As imaging is required at a minimum frequency, such as once every 30 seconds for neutrophils, this method cannot be scaled indefinitely due to the physical limitations of the microscope stage. In spite of using advanced algorithms for image registration and cell tracking, the limited speed of the stage places a constraint on the number of experiments that can be performed in parallel.
2. **Requirement of specialized equipment to run experiments** – Most microfluidic assays require the use to specialized equipment such as syringe pumps and stage-top incubators that both increase the labour to run a single experiment as well as increase reagent use and sample wastage.
3. **Heterogeneity and rare cells** – It is desirable that a microfluidic assay be able to work with rare cells in a population sample. These cells may be present in a cell sample at

extremely low densities (10-20 per ml), as in the case of circulating tumor cells in whole blood. While technologies to enrich these CTCs from whole blood has been developed using biological and biophysical techniques, current cell alignment or trapping techniques are not designed to work with such samples at a low density.

To address the fundamental limit to scalability in continuously tracked microfluidic chemotaxis assays, end-point analysis has been suggested as an alternative. In an end-point analysis chemotaxis assay, information regarding migration could be extracted from a single image at the end of the assay in a fashion similar to gel electrophoresis. Cell alignment in microfluidic devices is critical to developing end-point chemotaxis assays. In a scenario where all the cells in the device start migrating from the same starting line, a simple image at the assay end-point would be sufficient to obtain parameters like mean velocity and average displacement of cells.

2.4 Cell alignment in microfluidic devices

The ability to fabricate features in microfluidic devices that are of the same scale as biological cells enables the development of cell alignment/trapping functionality. Once aligned or trapped, biological cells can be independently treated or cultured and later analyzed. Each trap can also be subject to different physical or chemical conditions, resulting in a high throughput experiment. Alignment along a deterministic, well-defined array is a pre-requisite of experiment automation.

Cells aligned along a well-defined feature in the device are crucial to realizing end-point chemotaxis assays. Cell alignment in microfluidic devices can be achieved through various

means. This section will broadly explore some of the ways to do so and compare the advantages and drawbacks of each approach.

2.4.1 Hydrodynamic flow-based alignment

This method of alignment of particles and cells in microfluidic devices specifically relies on hydrodynamic flows in these channels and networks. As previously mentioned, flows at these length scales fall under the laminar flow profile and are deterministic as a result. This feature can be leveraged through device design to achieve cell alignment or trapping. The various techniques used to align cells hydrodynamically include –

2.4.1.1 Serpentine networks

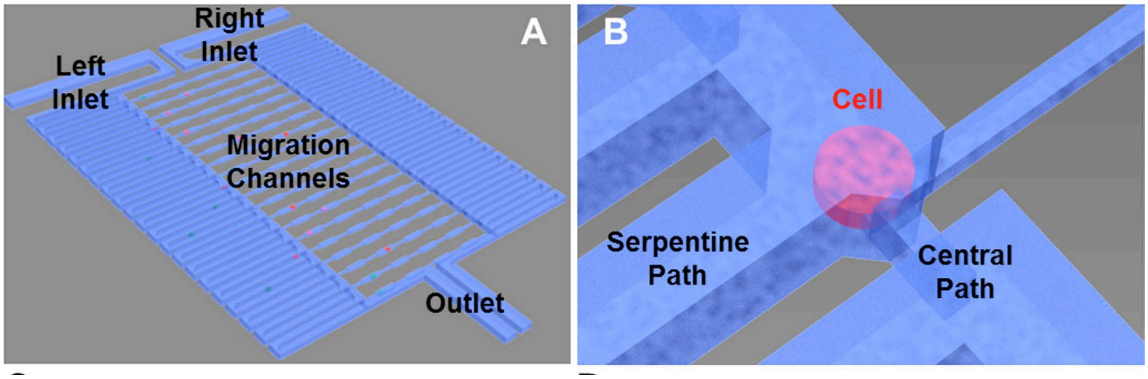

Figure 2.11 Serpentine channel network designed to trap cells in a microfluidic chemotaxis device[37]. Cells and fluid are added to the left inlet. The fluid is routed through the serpentine path when the cell blocks the central path, which has lower resistance. Though the central path is small enough to be able to trap cells, the serpentine path is designed to be long enough that the latter has a higher resistance. Reproduced with permission.

Serpentine networks utilize the principle of the path of least resistance to achieve cell trapping. Fluid flow is observed to be highest along the path of least resistance. If the path of least resistance is blocked, the fluid is routed around to establish a new path of least resistance. In serpentine networks, the source channel consists of a central path of low resistance which contains features to trap cells. It also has serpentine bypass channels for fluid to flow when the central path is blocked by a trapped cell. As a result, cells can consecutively be trapped at each junction of the central and serpentine path. While this method is highly deterministic, there is a clear upper limit on the number of cells that can be trapped in one device. Scaling the device to handle larger numbers of cells can only be done up to a certain point due to the requirement for larger pressure sources to establish flow. These factors place constraints on the cell density in the sample. Additionally, the cell cytoskeleton is under stress for the duration of the cell trapping process, which could affect its chemotactic ability.

2.4.1.2 Cup shaped traps

These traps have cup shaped features designed to trap cells. These traps place lower stress on the cell as compared to the serpentine channels. However, this technique also has a lower trapping efficiency in comparison.

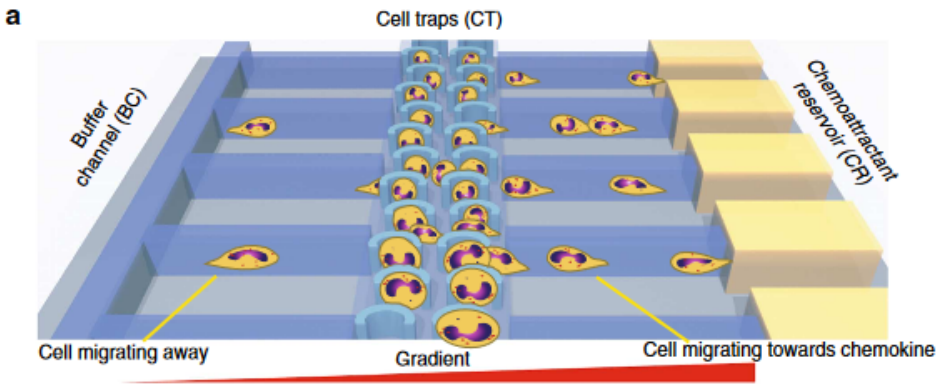

Figure 2.12 Cup shaped cell traps in microfluidic devices[40]. Reproduced with permission.

2.4.1.3 Perfused parallel dam

Parallel dam based designs utilize a fluid crossflow to dock cells against cells against a dam feature that lets fluid through but blocks cells. The crossflow is critical to achieve a monolayer of cells as seen in Figure 2.13. This design principle can also be combined with the perfused source sink gradient generation method to load the cells at a docking structure right next to the gradient channel[38].

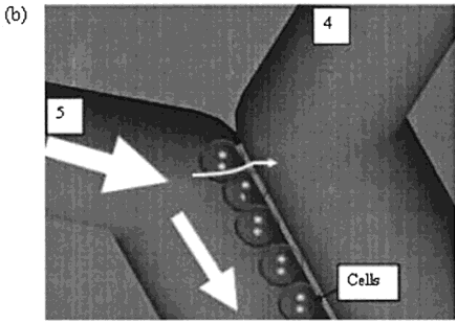

Figure 2.13 Perfused parallel dam alignment. The channel on the left is a higher pressure to ensure cell docking. Additionally, there is a cross flow to prevent cell accumulation that may block the channel. Reproduced with Permission

2.4.2 Centrifugation based alignment

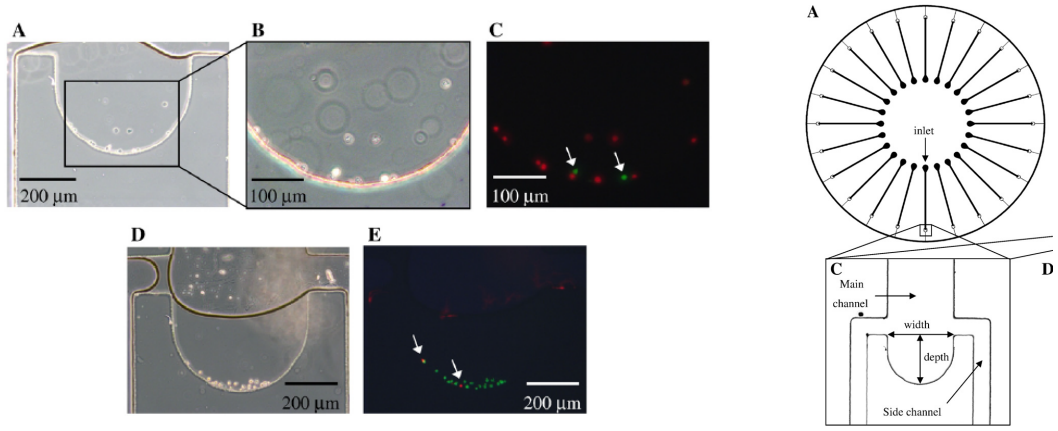

Figure 2.14 Centrifugal based alignment[42]. Cells are added into a radial device, which is subsequently spun to centrifugally trap/align. Reproduced with permission.

This technique aligns cells based on the application of centrifugal forces that push higher density particles in fluids away from the center of rotation. This method can easily be integrated with CD microfluidics devices. In prior work published using this technique[42], researchers loaded Jurkat cells into devices and spun them at 4500rpm for 60 seconds. As cells posess higher density in comparison to the surrounding fluid, centrifugal force results in their relative displacement to the fluid. The channel network is so designed that the cells are collected in a concave depression, while the excess fluid leaves the channel through side channels. Fresh media or various reagents could be introduced to the cells using this technique. This enables immunostaining and culturing of single cells in isolated conditions.

2.4.3 Surface functionalization-based alignment

Cells could also be aligned and captured in microfluidic devices using surface treatment techniques. Inspired by the process of neutrophil recruitment in the body, wherein rolling neutrophils are bound to P-Selectin expressed on the endothelial surface, the protein was

deposited selectively on to microchannels using microcontact printing. Neutrophils were found to exhibit similar behavior in vitro by selectively binding to the areas where P-Selectin was printed[43]. Neutrophils at a low density in the liquid solution could also be enriched in concentration under conditions of oscillating flow.

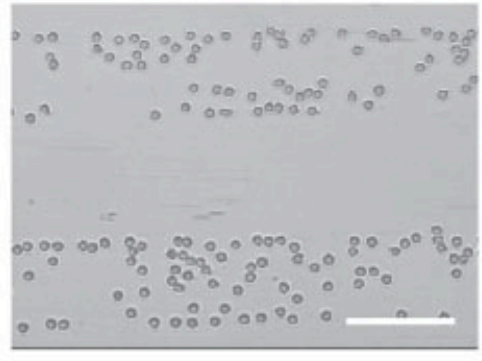

Figure 2.15 Cell alignment through surface functionalization and binding. The underlying surface is functionalized through microcontact printing using PDMS. Reproduced with permission.

Chapter 3: Design and development of end-point chemotaxis. assay

In this chapter, the pathway towards the development of a simple, scalable microfluidic chemotaxis assay with end-point analysis will be presented. Section 3.1 covers the goals and expected outcomes of such a microfluidic device. Section 3.2 introduces the concept of passively generated chemical gradients. The device design is presented in Section 3.3. Section 3.4 shows the results from fluorescence imaging of the gradient in the microfluidic device and simulations. Cell alignment achieved through centrifugation is discussed in Section 3.5. Section 3.6 documents towards efforts to build a microfluidic chemotaxis device integrating hydrogels, featuring a novel method to generate chemical gradients. This hydrogel microfluidic device was not used for subsequent experiments with neutrophils.

3.1 Microfluidic device design – Goals and constraints

The microfluidic chemotaxis device with end-point analysis is desired to have the following features

- Passive gradient generation with a small volume of chemoattractant. The generated gradient must also be stable against distorting forces of evaporation and flow.
- Cell alignment. The device must include features that are capable of aligning cells before cell migration.
- Ease of use – The experimental setup does not need to be linked to external equipment. Rather, it functions in a standalone fashion.
- Feasibility for high-throughput scaling.

These constraints and required features have important implications on the choice of the design of the microfluidic channel including the material, fabrication methods and experimental conditions. The subsequent sections will analyze and prototype the various material and fabrication options, gradient generation and cell alignment techniques.

3.2 Gradient generation in a passive source sink configuration

Figure 3.1 Passive source sink chemical gradient concept. The gradient channel functions to limit chemical flux. The reservoirs (source, sink) function to maintain a fixed concentration at either end of the gradient channel.

The source sink configuration to generate passive gradients in microfluidic devices is based on the dual principles of diffusion and hydrodynamic stretching of interfaces in pipe flows[44]. The configuration consists of source and sink reservoirs connected by a thin gradient channel as seen in Figure 3.1. The volume of the reservoir is orders of magnitude higher than the gradient channel. The source reservoir is initially filled with the chemical source, while the sink reservoir and the gradient channel are filled with buffer solution (Figure 3.1). As a result of diffusive flux, the chemical molecules diffuse from the source reservoir into the gradient channel creating a gradient. The role of the reservoirs is to maintain a fixed chemical concentration at the ends of

the gradient channel ensuring a quasi-stable gradient. By designing the reservoirs to hold a much higher volume than the channels, the gradient can be maintained for a long duration.

The diffusive flux in the device depends on the diffusion constant of the chemical as well as the geometry of the device. A shorter gradient channel results in larger flux but a shorter time to set up the gradient. According to Fick's law of diffusion, the mean diffusion distance of fMLP in water is 500 μm for 5 minutes. As the diffusion distance as the square root of time, the same molecule takes 4 times longer to diffuse over 1000 μm. This results in a long wait time to set up a stable gradient between the source and sink reservoirs.

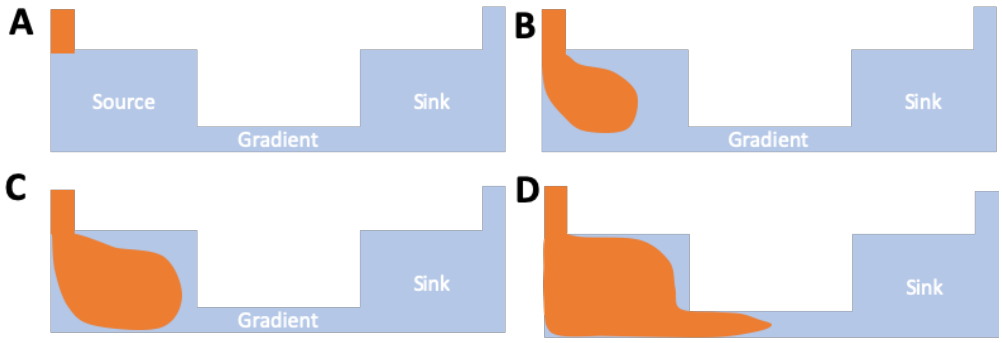

Figure 3.2 Taylor dispersion occurring during pipetting. Due to the parabolic flow profile resulting within the gradient channel, the interface between the chemoattractant (orange) and the buffer (blue) is stretched out leading to an increased effective diffusion.

However, diffusion is not the only fluidic phenomenon that occurs in a passive source sink configuration. Taylor dispersion arising from the loading process (Figure 3.2) stretches the interface between the chemoattractant and buffer as a result of the parabolic flow profile. A schematic illustration of this phenomenon is shown in the 4 panels in Figure 3.2. As a result of the Taylor dispersion and convective flows, the gradient stabilization occurs much faster than the

scenario with only passive diffusion from the source reservoir. This effect was later simulated using COMSOL Multiphysics and experimental gradient data through fluorescence used to confirm the generation as well as stability of the gradient. The results are presented in section 3.4.

3.3 Device design and fabrication

The passive source sink device was designed and fabricated in the form of a single layer PDMS device bonded to glass. Thorough extensive design and prototyping it was established that the device features such as cell alignment could be integrated with this basic design, enabling a single layer fabrication. This greatly simplifies the fabrication process as it does not involve any multilayer fabrication processes or alignment steps. The device design was parameterized based on the volume of the source and sink reservoirs, as well as the length and thickness of the gradient channel.

As mentioned previously, the geometry of the device, and the relative volumes of the reservoirs and gradient channel has a strong influence on the stability and longevity of the chemical gradient. Additionally, the geometry of device influenced the ease with which devices could be filled without generating bubbles. Once the individual device designs were tested and optimized to identify suitable dimensions that met these criteria (Figure 3.3), the individual device was duplicated and arranged in a radial fashion on a larger 2” by 3” substrate.

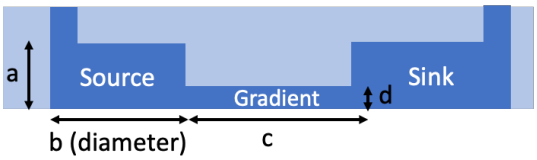

Parameter	b (mm)	c (mm)	d (um)	Volume
Device A	2	1	200	25uL
Device B	2	1	400	~25uL
Device C	3	1	200	57uL
Device D	3	1	400	~57uL
Device E	2	2	200	25uL
Device F	3	2	200	57uL

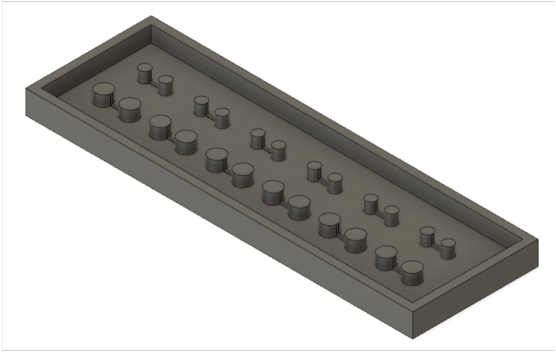

Fits on 1" by 3" glass slide

Figure 3.3 Passive source sink device optimization. Various dimensions of the reservoirs, length and height of the gradient channel were parametrized and tested to identify the optimal dimensions based on ease of filling, reagent use and the expected duration of the gradient generated.

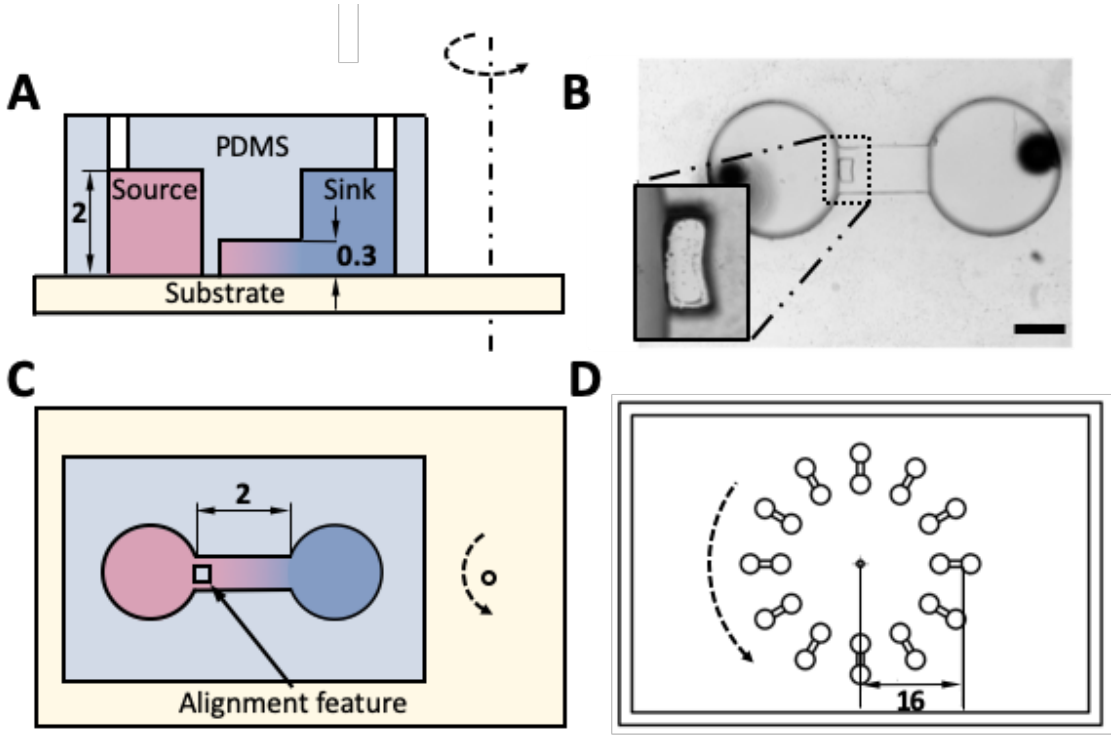

Figure 3.4 Design of the multiplexed end-point chemotaxis assay. (A) Cross-section of the microfluidic device design for an individual chemotaxis assay. Chemoattractant gradients are generated by passive diffusion

from a reservoir. (C) Top-view of the microfluidic device showing the alignment barrier and critical device dimensions (in mm) (B) Micrograph of an individual chemotaxis assay. Scale bar = 1000 µm. Inset: Concave barrier for cell alignment. (D) Design of the 12-plex end-point chemotaxis assay where cell alignment is achieved through centrifugal alignment.

A microscope image of the fabricated device can be seen in Figure 3.4B, where the alignment barrier feature has been shown in greater detail to highlight the concavity in its design. This concave feature is used to stabilize cells during alignment as well as reduce shear stress. Figure 3.4D shows the arrangement of individual devices in a radial fashion around the center of the substrate. The alignment feature in each device is located 16mm away from the axis of rotation.

3.4 Passive gradient simulation and validation

To quantify and validate the chemoattractant gradients generated in the microfluidic device, we performed finite element simulations and experimentally confirmed them by imaging equivalent gradients of fluorescent molecules (FITC-Dextran). Simulations were performed to first understand the extent of flow dispersion caused due to pipetting the chemoattractant solution into the device. The effect of diffusion on the initial gradient formed by dispersion was also simulated over a 3-hour time period. The results are seen in Figure 3.5 where the gradient was found to substantially evolve and strengthen over this time (dashed lines). This validated our hypothesis that a sufficiently thin microchannel limiting diffusion between two reservoirs at different concentrations can maintain a stable gradient over a long period of time.

To visualize the gradient for experimental analysis, FITC-Dextran (10kDa) was chosen as the fluorescent molecule. Evaporation and pressure differences between the inlet and outlet are known to generate undesirable flows that distort the gradient. To eliminate these effects, inlets were covered using silicone oil during experiments. The gradient profile in the microfluidic gradient channel is linear in the vicinity of the alignment barrier (Figure 3.5B, Solid lines) and is strengthened as well as stabilized with time (Figure 3.5C). Eliminating evaporation as well as pressure differences using silicone oil is also found to be a viable alternative to design strategies such as shunt channels for eliminating gradient distortion due to flow. Generating a gradient that could be sustained for over 3 hours only required 5 μL of the chemoattractant solution. The device is capable of generating stable gradients using only a small volume of reagents and no external instrumentation.

To determine the effect of the alignment barrier on the gradient, we performed simulations of the device with and without the alignment barrier. As shown in Figure 3.5D, the presence of the alignment barrier reduced the gradient strength (solid plots) in its vicinity as compared to the channels without such a barrier (dashed plots). This reduced strength occurs as a result of greater diffusion in a constrained geometry. The presence of the alignment barrier is found to marginally decrease gradient intensity at the barrier.

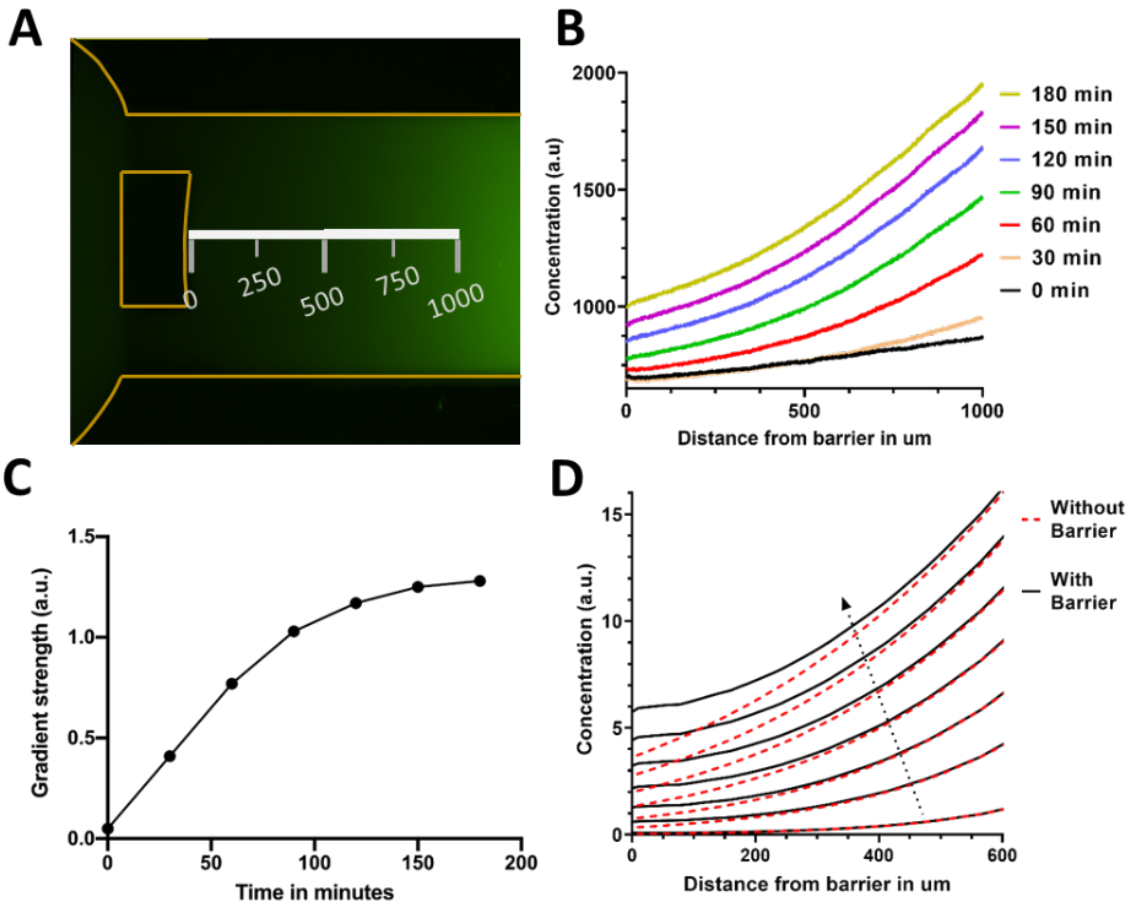

Figure 3.5 Gradient generation using passive diffusion. A: Fluorescence micrograph of the chemoattractant gradient as visualized using FITC-Dextran (green). Positions along the channel in the context of figure C and D are also shown. B: Concentration profile along the channel as observed through fluorescence microscopy C: Gradient strength at the alignment interface measured experimentally as a function of time D: Effect of alignment barrier causing higher mixing and resulting in a weaker gradient.

3.5 Cell alignment through centrifugation

To align cells in this device, we developed a centrifugal alignment approach where cells that have a higher density as compared to the surrounding liquid medium in the microfluidic channel

are pushed outwards due to centrifugal force when the device is spun. Cells moving relative to the surrounding fluid also experience a drag force (F_d), which balances the centrifugal force (F_c), resulting in a constant terminal velocity or sedimentation rate. This velocity or sedimentation rate depends on the rotational speed as well as the position of the cell within the channel. The various forces on the cell are summarized in Figure 4.5F. To stabilize the aligned cells against Euler forces (F_e, Figure 4.5F), arising from spinner ramp cycles the barrier feature was designed to be concave. The concave feature helps in reducing the inertial shear stress on the aligned cells during the spinning process.

The transport of cells in the microfluidic device via centrifugation was modelled under conditions of Stokes flow. Specifically, neutrophils can be considered as spheres 5 μm in radius (R) with a density (ρ) of 1.08 g/ml[45]. The dynamic viscosity (μ) of the cell migration media was considered to be similar to that of water at 25 degrees Celsius. Under conditions where the drag force (F_d, Equation 4.2) under stokes flow conditions were balanced by the centrifugal force (F_c, Equation 4.1), the average sedimentation rate (v) is proportional to the square of the rotational speed (ω) as well as the distance from the axis of rotation (r) (Equation 4.4).

Equation 3.1 Centrifugal Force

$$F_c = m\omega^2 r$$

Equation 3.2 Drag force under Stoke's Flow

$$F_d = 6\pi\mu R v$$

Equation 3.3 Sedimentation rate

$$v = \frac{2\rho R^2 \omega^2 r}{9\mu} = k\omega^2 r$$

At a rotation speed of 1500 rpm, the sedimentation velocity was calculated to be 225 μm/s near the alignment barrier and lower at positions closer to the axis of rotation. At this speed, a cell at the edge of the inlet reservoir would take around 20 seconds to traverse the 4000 μm distance to the alignment barrier. This would result in the alignment of a majority of cells in the device in under a minute, accounting for the spinner ramp up and ramp down time as well.

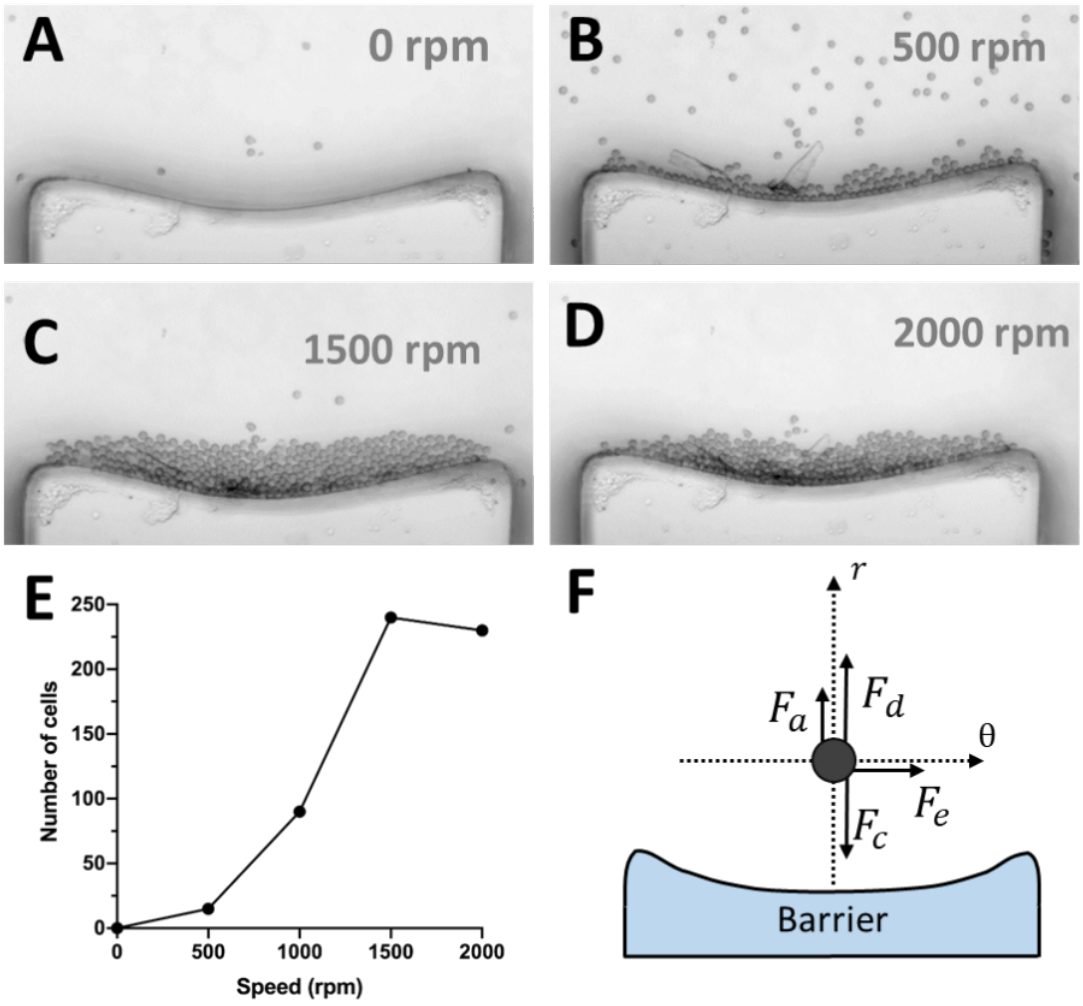

Figure 3.6 Cell alignment through centrifugation. A through D Effect of centrifugal alignment on the alignment of the cells at various spin speeds. There are progressively more cells in 3B (500 rpm) and 3C (1500 rpm) as compared to #A (0 rpm, before spin). E) Spinning at higher speeds results in fewer aligned cells due to limited concavity of the barrier as seen from D and E.

To establish the feasibility and efficacy of the centrifugal cell alignment process, we loaded the microfluidic device with human neutrophils and spun the device at several speeds. The spinner was always set to the lowest acceleration ramp setting of 100 rpm/sec to minimize Euler forces. After spinning, we used microscopy to determine the number of cells aligned to the barrier feature, as well as those remaining in the channel. While spinning the device at 500 rpm provided enough centrifugal force to overcome the adhesive forces (F_a), spinning for a minute aligned only a small fraction of cells due to the low sedimentation rate. Cell accumulation after 60 seconds of spin time at higher speeds up to 2000 rpm is shown in Figure 3.6A-E. At speeds higher than 1500 rpm, cells that are not adequately shielded by the concave alignment barrier were found to be displaced by the tangential forces arising from the spinning process.
In summary, rotation at 1500 rpm for one minute in our device was found to be the optimal speed to align neutrophils. The concave alignment barrier was found to be effective in stabilizing aligned cells within the device.

3.6 Passive gradient generation through controlled release from PEGDA hydrogels

3.6.1 Introduction

This section introduces a novel method to generate passive gradients using hydrogels. Due to a lack of adhesion between the cells as the underlying hydrogel substrate, chemotaxis could not be observed within this device. The concept of hydrogel generation, multilayer PDMS device fabrication and suggested solutions to PEGDA adhesion are discussed.

3.6.2 Hydrogel gradient generation concept

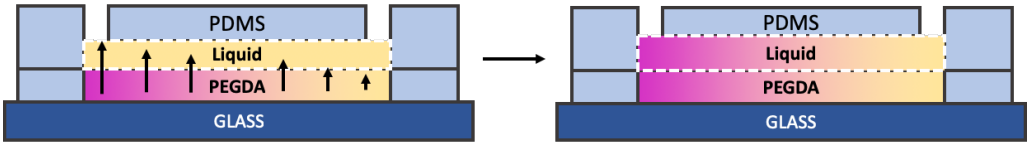

Figure 3.7 Concept for gradient generation through the use of hydrogels. Polyethylene Glycol Diacrylate (PEGDA) is polymerized with the desired gradient, which generates a secondary gradient in the liquid above the hydrogel.

A simplified cross-sectional schematic of a device wherein the chemical gradient is generated through controlled release from a Hydrogel is shown in Figure 3.7. Controlled release of chemicals from hydrogels have been used to develop slow release medication[46] as well as generate gradients in microfluidic channels[11]. In this mode of operation, a desired chemoattractant gradient in the liquid pre-polymer solution is "frozen" by hydrogel polymerization. This polymerization results in a decrease in the diffusion constant of the chemoattractant within the hydrogel. This occurs as a result of interactions between the solute molecule and the polymer matrix of the hydrogel decreasing the mean free path of the solute molecules as well as the diffusion coefficient[47]. When the polymerized hydrogel is covered by buffer liquid, the gradient in the hydrogel is projected on the liquid at the interface through a process of diffusion.

The gradient generated through controlled chemical release from hydrogels was simulated using finite element modelling and demonstrated to be linear (Appendix A.1). However, the liquid was also found to leach the hydrogel interface of chemical, reducing the strength of the gradient.

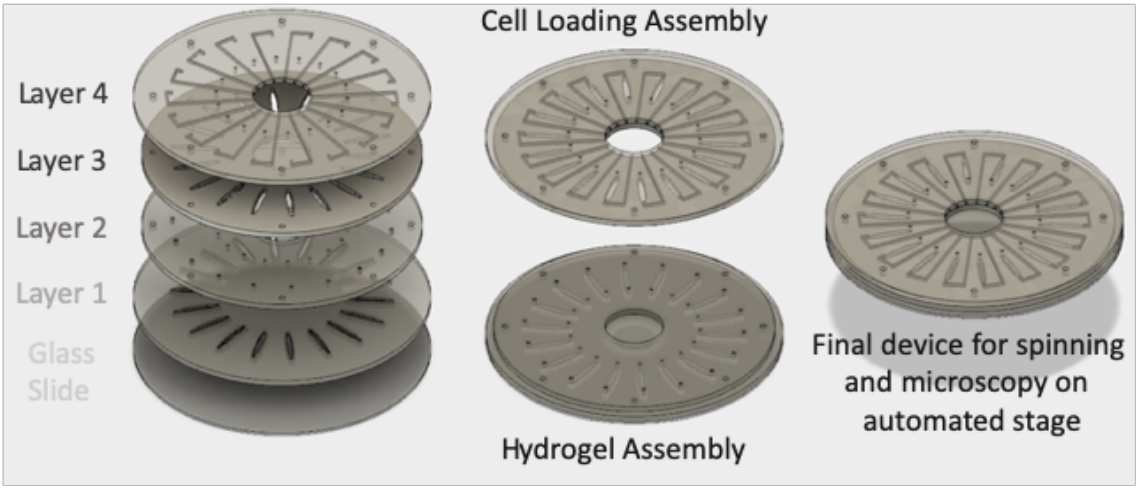

Figure 3.8 Multilayer hydrogel PDMS device fabrication process. Five through-cut layers of PDMS are aligned and bonded on to a glass slide to create the final device to be spun and placed in the incubator for migration to occur.

Integration of hydrogels into a PDMS device necessitated a new approach for device fabrication and assembly of the entire device. In traditional PDMS devices, bonding of PDMS layers to other surfaces such as glass or PDMS is done through plasma bonding. This technique could not be used in the case of this device after hydrogel polymerization as plasma bonding cannot take place in the presence of moisture and water content. As a result, novel solutions to achieve through-cut PDMS layers, multilayer PDMS bonding and alignment are described in Appendix B to fabricate a device as shown in Figure 3.8.

3.6.2.1 Results and discussion

To verify cell migration in hydrogel devices with gradients of fMLP, differentiated HL60 cells (dHL60) on day 5 were added to PDMS devices in which 100 nM fMLP gradients were created

using the hydrogel technique. Cells in each device were imaged at 30 second intervals for 2 hours. TrackMate[48] was used to track and visualize cell paths.

dHL60 cells on a PEGDA hydrogel did not respond to gradients of fMLP. This direction and nature of cell movement was not found to correlate with the gradient. Moreover, on observing different locations in the same device it was found that cells were moving in different directions as seen in Figure 3.9. Overall, cells were found to move to the middle (along the channel length) where they were also found to collect. The movement of cells from the barrier alignment feature was also found note correlate with the applied chemical gradient. Sealing the device with silicone oil eliminated all possible sources of external factors causing this flow, establishing factors internal to the device as the cause for this anomalous behavior.

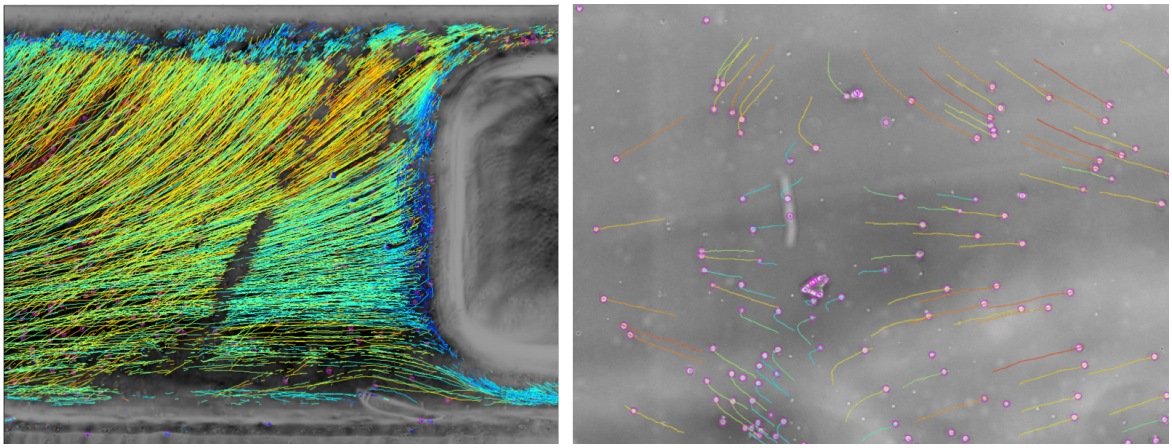

Figure 3.9 Cell migration on PEGDA hydrogel surfaces showing extensive movement and collection regions. The denoted lines show the cell paths over a 15-minute observation period. The color denotes the average speed of the cell tracks.

To further understand the cause and nature of cell collection, the experiment was repeated with fixed cells as well as BSA-blocked beads. Similar results were observed, leading to the

conclusion that the observed motion was due to physical effects causing local, internal flows in the device and not any cellular processes. It is suspected that the absence of equilibration step for the Hydrogel leads to flexure of the substrate the cells settle on as well as fluid absorption[49]. Due a lack of adhesion of cells to unfunctionalized PEGDA surfaces, cells could freely move on this undulating substrate, leading to the observed results.

Therefore, the lack of a chemotactic response could be explained in part by the lack of adhesion to the underlying substrate. To increase substrate adhesion to neutrophils and other cells, the PEGDA hydrogel could be replaced by other biologically derived polymers such as matrigel[50]. PEGDA hydrogels could also functionalized with peptides such as RGDS[51] to increase adhesion. As such, the focus shifted to other substrates that could be modified to ensure neutrophil adhesion in a way similar to *in vivo* ECM adhesion. The chosen substrate is also desired to possess a uniformly flat surface for chemotaxis dominant migration to take place unhindered.

Chapter 4: Chemotaxis in the PDMS microfluidic device

Chemotaxis results with human neutrophils will be introduced in this section. Section 4.1 lists the detailed protocols developed to coat the device with the desired ECM protein and subsequent BSA blocking. Protocols for neutrophil separation, handling and device centrifugation are also mentioned. Results from both continuous time-lapse microscopy as well as end-point analysis will be discussed in sections 4.2.3 and 4.2.4. To conclude, a pathway for future device development is presented.

4.1 Materials and methods

4.1.1 Device fabrication and assembly

- 30 grams of PDMS (Sylgard 184, Dow Corning) was mixed according to the manufacturer's specifications, degassed and poured into the 3D printed mould (Protolabs, Raleigh, USA)
- The PDMS is heat-cured at 65 C for 2 hours and stored at room temperature until ready to be used.
- Cured PDMS layer is peeled off the mould and inlet holes are punched in the source and sink reservoirs using a 1mm hole punch
- The device is then bonded to a pre-cleaned 2" by 3" glass slide (TedPella Inc, USA) using a plasma cleaner (Harrick Plasma PDC-001). Both surfaces were plasma cleaned a high setting for 90 seconds. The ECM protein coating solution was immediately added to the channels within 5 minute of plasma activation.
- In the event that bubbles form in the reservoirs, they can be removed by filling the device with excess solution and gently pressing down on the reservoirs using a 1ml pipette. This

results in the bubble being pushed out of the device. When the reservoir is allowed to release up, it fills up with the liquid surrounding the inlet.

4.1.2 Cell preparation

- 5ml of whole blood was collected from healthy human volunteers in EDTA tubes.
- A neutrophil isolation kit (Stemcell Technologies, Vancouver, Canada) was used to enrich the whole blood sample of neutrophils using the manufacturer's protocol.
- Resulting neutrophils were resuspended in RPMI-1640 supplemented with 0.4% BSA. Cells were stored inside the incubator at 37 degrees and used within 2 hours of neutrophil separation.

4.1.3 Device preparation, cell loading and alignment

- 20 μL of the chosen ECM protein solution (diluted down to the chose concentration in PBS) was immediately pipetted to the plasma activated devices
- After 1 hour, the ECM protein solution was flushed out of the device with PBS and replaced by a solution of RPMI 1640 with 0.4% BSA. BSA blocking was done for one hour.
- Neutrophil solution containing cells was then added to the device
- At this stage, excess solution on the PDMS device was wicked away using Kimwipes, resulting in a dry outlet region over the sink reservoir. A piece of laser cut acrylic tape was then placed on the outlet hole to seal it in preparation for the cell alignment process

- The device assembly with sealed outlets was transferred onto a Headway spinner where it was spun at 1500 rpm for 60 seconds. The lowest acceleration settings were chosen to minimize Coriolis forces
- After visual confirmation of cell alignment, the device is then transferred to the incubator for 15 minutes to allow for the cells to adhere to the ECM-protein coated glass substrate
- The tape blocking the outlets was gently peeled off, and 5 μL of chemoattractant solution was introduced into the source reservoir
- After removing excess fluid at the outlet and ensure a dry surface, a thin layer of silicone oil was applied to minimize evaporation and eliminate any resulting flow
- The device was placed in a custom laser-cut enclosure and transferred to the microscope stage holder for continuous microscopy or the incubator for subsequent endpoint analysis.

4.1.4 Imaging and analysis

- The X, Y and Z locations of the barrier features in each of the 12 devices are stored in the imaging software (NIS Elements AR) and offset after recording the position of the first device.
- A multi-lambda, multi-point time lapse acquisition protocol is designed to capture the gradient evolution as well as cell migration in each of the 12 devices at a 30 second frequency for 2 hours.
- The images were analyzed using the FIJI cell tracking plugin from ImageJ. The protocol for image analysis has previously been described in section 3.6.4 and was used without any modifications on the neutrophils.
- The XML files obtained from FIJI with cell locations were subsequently analyzed and plotted using Python

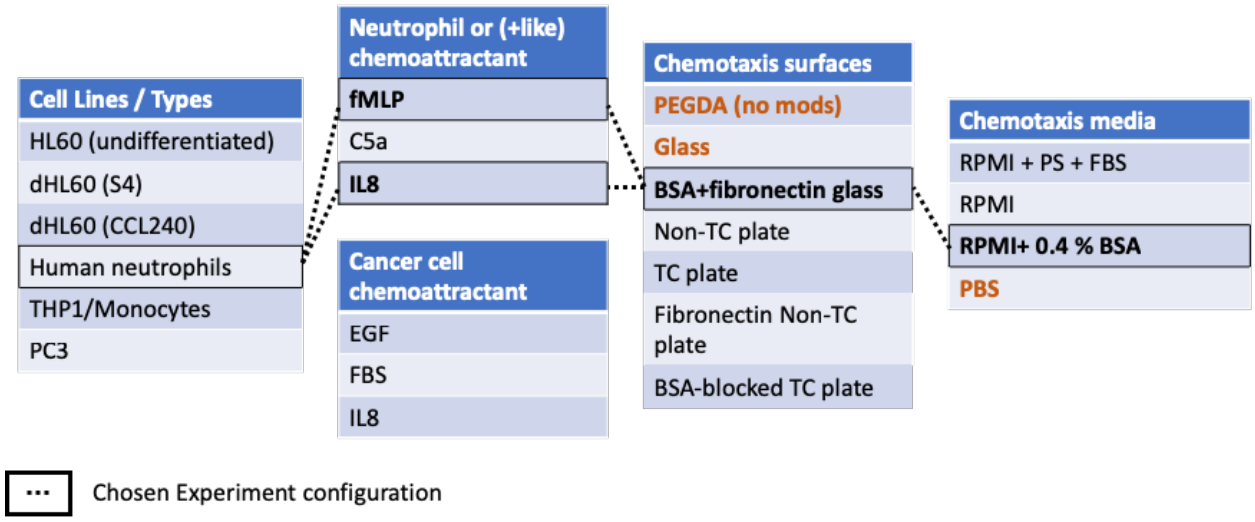

Figure 4.1 Experimental configuration-space visualized to show the various cell types, chemoattractants, surfaces and media considered and tested in the process of developing the microfluidic chemotaxis assay.

The various conditions in an experimental configuration were visualized in a form seen in Figure 4.1. This was useful for comparing various conditions between experiments.

4.2 Results and discussion

4.2.1 Acquired images and cell tracking

An overview of the data acquired through microscopy in a single experiment is shown in Figure 4.2. The microscope stage sequentially moves through the 12 devices on the substrate, taking both bright field and fluorescence images at each location. Imaging over a 2 hour duration results in a time-lapse video at a 30 second frequency.

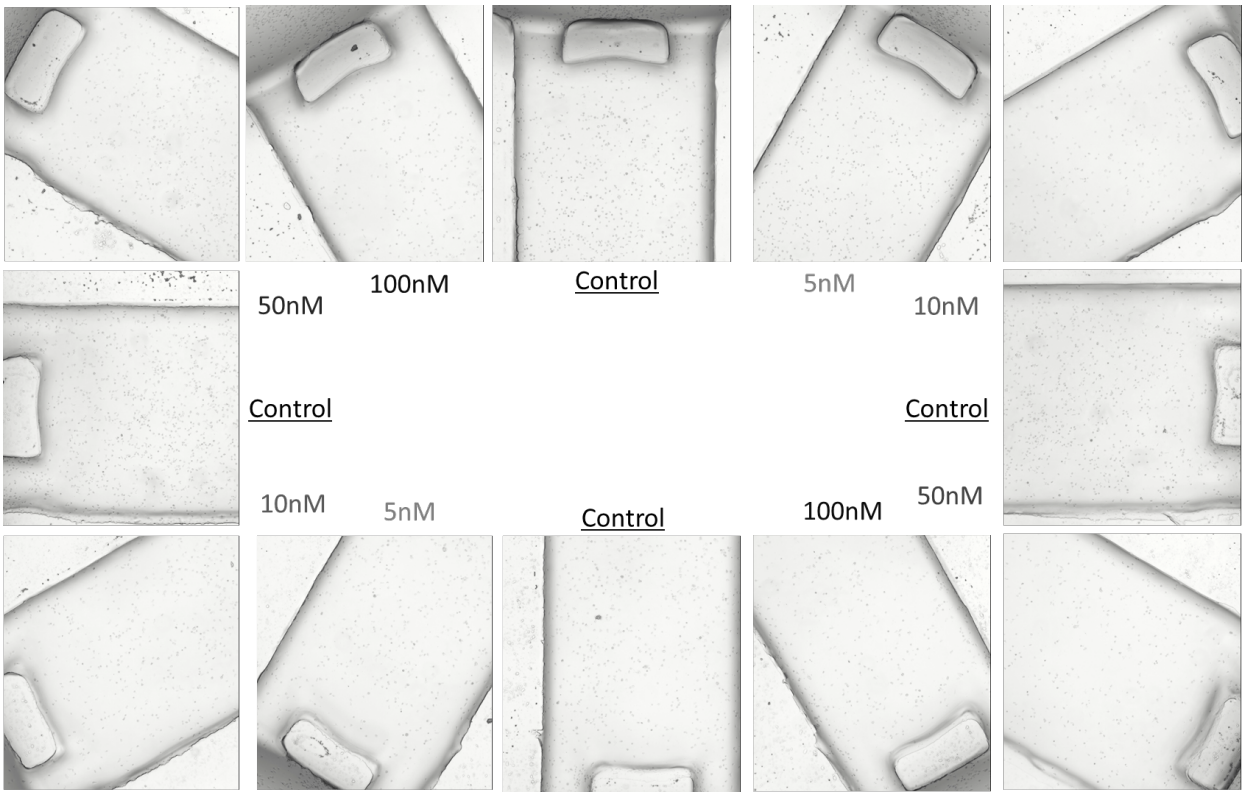

Figure 4.2 Output of the multi-wavelength, arrayed time lapse imaging protocol showing images obtained from each of the 12 channels in the microfluidic device. Each image is rotated in multiples of 30 degrees to obtain a horizontally-oriented imaged which is later analyzed.

The image of each device is inverted and rotated by its respective angle to ensure similar conditions across devices and compatibility with the cell tracking plugin. Since the plugin is only capable of segmenting sections of the image that are brighter than the background, the bright field images are inverted. The images are then segmented to identify cells within a desired section of the image. An automated cell tracking algorithm from the TrackMate plugin [48] is used to produce the cell paths. An overview of this process can be seen in Figure 4.3. The raw cell paths in XML format are then exported to be later processed using a custom python script.

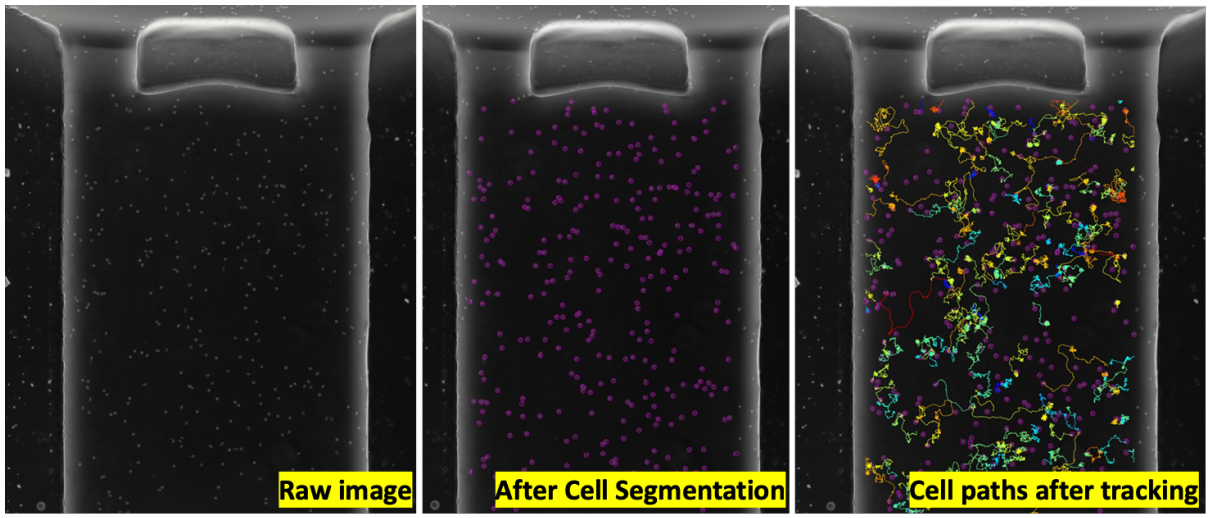

Figure 4.3 Process of image analysis using the ImageJ TrackMate plugin. Raw images are inverted to ensure compatibility with cell tracking software. Each frame is segmented to identify cells. Image registration is performed to track cells between consecutive frames using the TrackMate plugin in imageJ.

4.2.2 Data analysis and visualization

The raw cell paths are analyzed to calculate parameters such as mean velocity, mean displacement and mean directness, which is the ratio of the displacement to speed averaged over each individual cell. A directness value of 1 would imply that cells are travelling along straight

lines, while a directness factor closer to 0 would be indicative of a meandering path. Since the directness values for the neutrophil migration was observed to be less than 0.5, only the final displacement vectors for the cells were plotted rather than the actual path for better clarity (Figure 4.4)

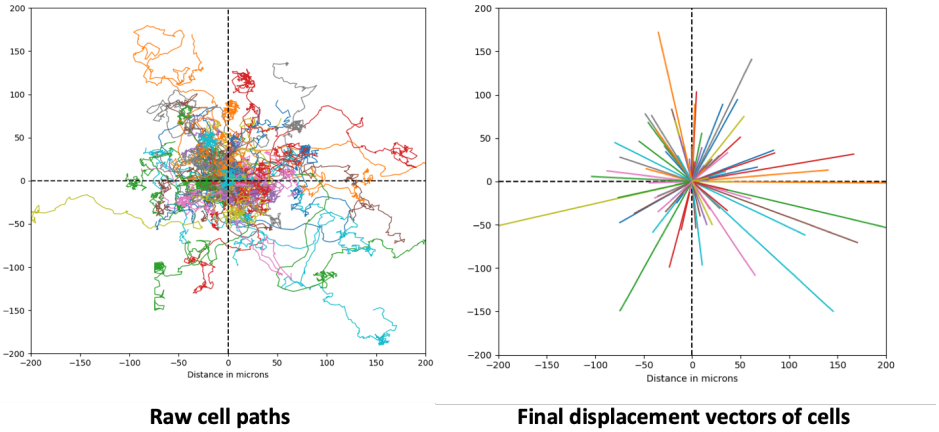

Figure 4.4 Sample raw cell paths and final displacement vectors of migrating cells extracted from XML files

4.2.3 Neutrophil migration in fMLP gradients (continuous microscopy)

To validate neutrophil chemotaxis in the microfluidic device, we performed chemotaxis assay in gradients of fMLP using human neutrophils. Neutrophils were isolated from whole blood using a commercial magnetic immunoselection kit and resuspended in a cell migration media. Cells were infused into the device after fibronectin coating and BSA blocking.

Cells in fMLP gradients had an elongated morphology in contrast to the rounded morphologies seen in control devices (Figure 4.5). Analyzing the cell tracks at an individual cell level revealed directional bias of Neutrophil migration in 100 nM fMLP gradients with 80% of all cells moving

towards the source of the chemoattractant. Neutrophils had an average migration velocity of 2 μm/min in 100 nM gradients. The cell paths were found to have an average directness factor of 0.3 (ratio of displacement to total distance). In contrast, control sample showed no net displacement and did not possess a directional bias. The developed device is therefore capable of eliciting a chemotactic response from neutrophils.

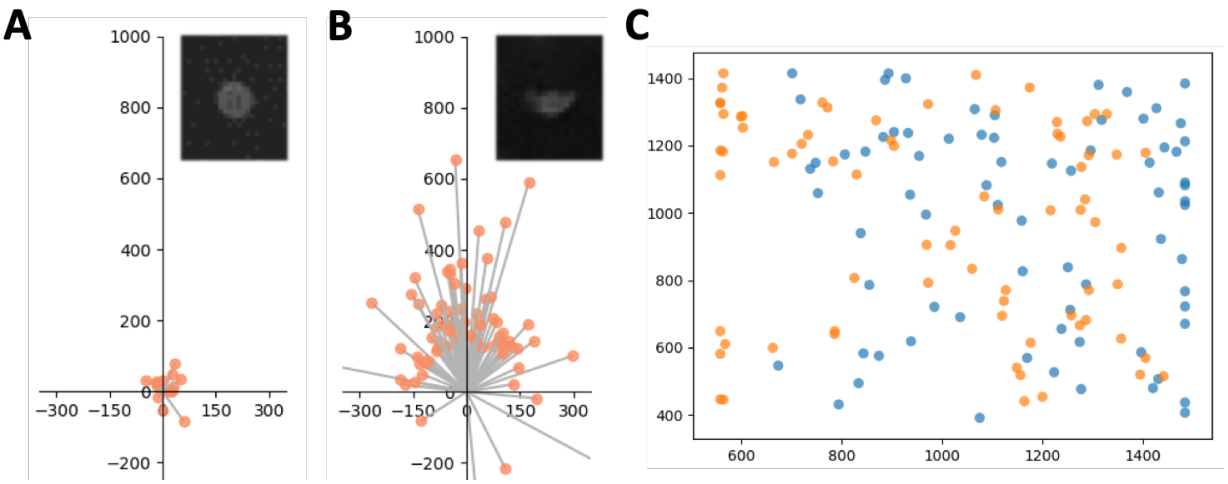

Figure 4.5 Validation of chemotaxis in the microfluidic device. A) Cell migration in devices without fMLP observed through real time tracking for 2 hours. Inset: Cell morphology is observed to be rounded B) Cells under the influence of a 100nM fMLP gradient showed directed migration in the direction of fMLP as well as elongated morphologies (Inset) C) Scatter plots showing cell positions before (Orange) and after (Blue) migration. The 100 nM gradient is applied from the left to the right.

4.2.4 Endpoint analysis chemotaxis assay

To establish the effectiveness of the end-point chemotaxis assay, we perform the same experiment as before on human neutrophils with the additional step of alignment via centrifugal sedimentation and observed the net migration of human neutrophils that were previously at the alignment feature after a fixed amount of time. Cells aligned against the feature were subject to a chemical gradient and the entire device assembly placed inside an incubator. The end point assay was validated by comparing the positions of neutrophils after 2 hours of migration away from the alignment feature under gradients of fMLP. Locations of cells were obtained by automatic segmentation of a microscope image of each device (Fig.4.15C). The distance of the cells from the alignment feature can be visualized as a cumulative distribution (Fig. 4.15D) or as a beeswarm plot (Fig. 4.15E). As seen in Fig. 4.15A, the majority of cells in the devices without fMLP possess rounded morphologies and can still be found in their original aligned positions. In contrast, cells subject to a 100 nM fMLP gradient have migrated away from the alignment feature and additionally have elongated morphologies (Fig. 4.15B). As observed in the cumulative distribution function (Fig. 4.15D), the medial position of the cell distribution is approximately 10 μm from the alignment feature in control devices while it is 150 μm in devices with fMLP gradients. The distribution of cells also captures the variability and heterogeneity in Neutrophil chemotactic response at a single cell level. The cell distributions in control and 100nM gradient channels show a statistically significant difference ($p<0.05$, Student's t test). The device is therefore capable of measuring the chemotactic ability of a cell population without needing continuous tracking.

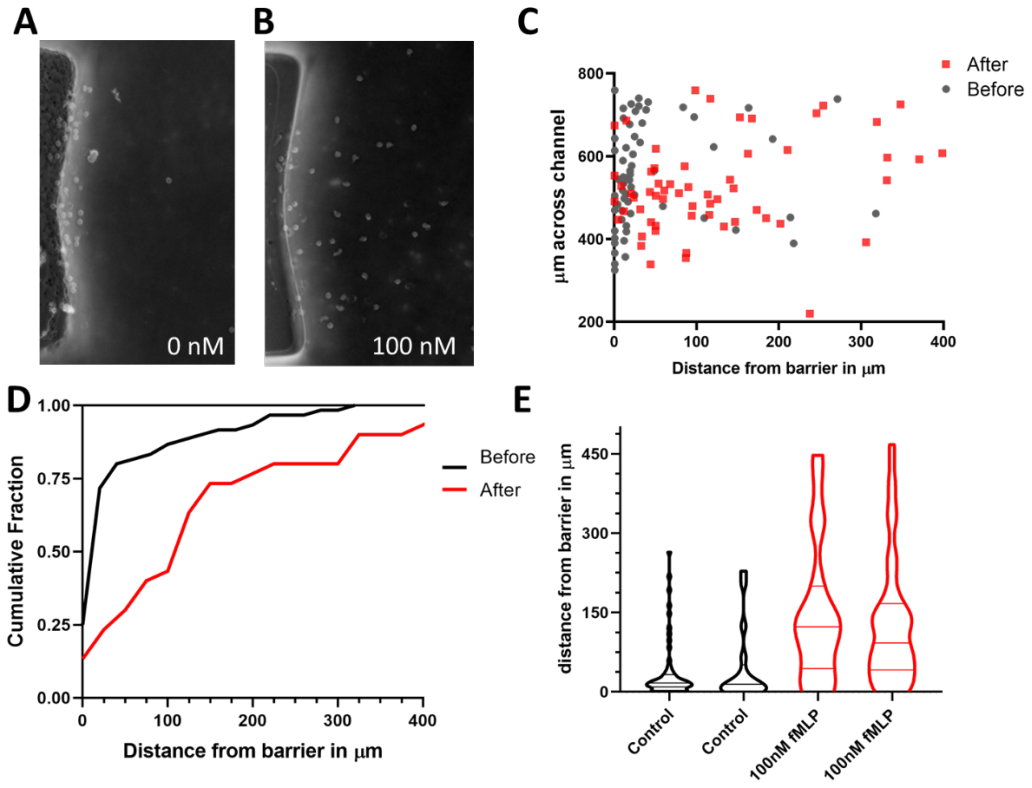

Figure 4.6 Endpoint analysis chemotaxis assay. A) Cell migration after alignment in a device without fMLP (Control) B) Cell migration in a device with an fMLP gradient showing cells positions after migrating away from the alignment barrier C) Comparison of cell migration after 2 hours between control (Orange) and 100nM gradient (Blue) D&E) Cumulative distribution functions and Beeswarm plots showing a statistically significant difference between cell response in control and fMLP gradient devices .

Chapter 5: Discussion and future steps

5.1 Discussion

In this study, we investigated an approach to develop a multiplexed end-point chemotaxis assay by aligning the cell sample against a barrier via centrifugation. The aligned cells are then exposed to a passively generated chemoattractant gradient, which causes the cells to migrate away from the barrier. After migration in an incubated environment, chemotaxis for each cell sample can be determined from a single microscopy image. Fluorescence imaging was used to observe chemical gradient profiles and validate its stability 3 hours after generation. Cell alignment at the barrier feature after centrifugation at various spin speeds was quantified through microscopy. Neutrophils in gradients of fMLP showed elongated morphologies and directed migration, while cells in control devices were rounded and non-motile. End-point analysis was used to obtain the average displacement of the cell population in response to the gradient as well as the spread in the final positions of cells after migration.

Live imaging of cells undergoing chemotaxis is a commonly used method to analyze cellular behavior. While it has the ability to describe cell behavior in great detail[52], there are fundamental limits to scalability in order to perform experiments in parallel. Previous studies have multiplexed chemotaxis assays using automated continuous microscopy to analyze up to 7 devices in parallel[53]. These studies were limited by the frequency of imaging set by the finite speed of the automated stage and the migration speed of cells. Rapidly moving cells, such as neutrophils, require an imaging frequency of 0.03 Hz (an image every 30 seconds) for optimal cell registration and tracking[13]. Other algorithmic approaches have increased experimental throughput to 50 devices by imaging at a lower frequency to capture the relative cell

displacement. Such approaches nevertheless require continuous imaging, where there is a risk of evaporation leading to convective flows and device to device variability[54 55].

Chemotaxis assays with end-point analysis provide a simpler approach to increase throughput by positioning cells at the same initial point. The average displacement of the cell population as well as the variability in migration can be captured through a single image at the assay endpoint since the initial positions of the cells are known. Studies have correlated parameters describing chemotaxis at individual cell level and those that model migration at population level[56]. While continuous microscopy is crucial in understanding cytoskeletal dynamics and locomotion during chemotaxis, the higher throughput offered by end-point analysis is more relevant to the application of drug testing and screening. Moreover, end-point assays also enable isolation and separation of chemotactic phenotypes in a cell population for downstream analysis[37].

Previous efforts to develop end-point chemotaxis assays patterned cells using traps and constrictions to position cells at their initial starting points. The cells must be transported into these locations using carefully controlled fluid flow, which is difficult to scale[53] and can require a large amount of reagents (up to 100 μL[35]). Aligning cells using traps and constrictions also applies significant shear stress on the cells, which can affect their migratory properties[57]. Additionally, the geometry of the traps or constrictions must be matched to the geometry of the cell as well as the density of the cell sample, which makes this approach less robust when dealing with heterogeneous samples, such as primary samples from patients. Our centrifugal alignment method provides an alternative approach for cell alignment that does not require precise flow control, applies minimal shear stress to cells, and is insensitive to cell geometry.

The device design has a small footprint leading to high-density on a single substrate therefore allowing for many experiments to be run simultaneously. The simple, single-layer device does not require external controls leading to simple operation and can be subsequently automated using a pipetting robot. Each individual device requires only a small amount (5 μL) of the chemoattractant solution at the desired concentration to generate the gradient. Centrifugation allows for simultaneous alignment of a wide range of cell types seeded at various densities. All these features result in a stand-alone multiplexed device which can simply be placed in the incubator where chemotactic migration can occur. A primary cell sample can be treated with various concentrations of different activation factors and drugs in separate devices to perform 100s of experiments in parallel.

In conclusion, we demonstrate that centrifugal alignment enables the development of a multiplexed end-point chemotaxis assay that is simple and easy to use. Our assay is suitable for scaling in order to fulfill the requirements for high-throughput screening studies

5.2 Limitations

In its current state, the assay requires further optimization for high throughput studies. As previously mentioned, the gradient is strongly dependent on the nature of flow profile while the chemoattractant solution is being injected into the device. This can be attributed to the flow velocity contribution to the effective diffusivity under conditions of Taylor dispersion. Manual

pipetting results in variability in gradient profiles that may affect the cell migration response. As such, the current method of gradient generation is not suitable for high throughput analysis.

The device is fabricated in Polydimethylsiloxane (PDMS) for ease of fabrication. Additionally, irreversible and strong PDMS bonding to glass substrates can be easily achieved through plasma oxidation. PDMS is however, a naturally hydrophobic polymer. As a result, fluid needs to be added to the device immediately after plasma activation to prevent bubble formation. Devices cannot be precoated with the desired surface treatment (Extra cellular matrix proteins). This increase the hands-on time for running experiments. Currently, each device requires almost 3 hours of benchtop handling before it can be placed in the incubator for migration to occur. This could be reduced to 30 minutes if pre-coated devices could be used.

The position of the barrier feature within the gradient channel also requires further optimization. In a few cases it was observed that cells in the sink reservoir in close proximity to the gradient channel, that are initially rounded and unpolarized, migrate with a high directionality in response to the gradient. As such the optimal position for the barrier feature is hypothesized to be at the interface of the gradient channel and the reservoir rather than being placed wholly within the gradient channel. This is however expected to introduce fabrication constraints that require further optimization.

5.3 Future Steps

So far, we have designed and validated a PDMS microfluidic device for the application of an End-point chemotaxis assay. The passively generated gradient has been validated for stability, and centrifugation has been demonstrated to be effective in aligning cells. The future steps suggested in this section are practical considerations and steps that required to fully realize the scalability of this chemotaxis assay.

5.3.1 Generating repeatable, accurate gradients with an automated pipette

The current method for passively generating chemical gradients is sensitive to the flow rate during pipetting as a result of Taylor dispersion. The extent and length of the parabolic flow profile depends on the speed with which chemoattractant solution is introduced into the channel. This in turn influences the effective diffusivity as seen in Equation 5.1, which depends on the device dimensions as well as maximum velocity of fluid. To ensure gradient repeatability across tens of devices on the substrate, it is crucial to load each device in a similar fashion without human variability. Therefore, an electronic pipette that is capable of dispensing an accurate volume at a fixed flow rate must be used to achieve repeatability across experiments.

Equation 5.1 Effective diffusion during Taylor dispersion

$$D_{eff} = D + \frac{a^2 {u_{max}}^2}{192D}$$

5.3.2 Contactless dispensing

The device is currently designed in such a way that contact between the inlets and pipette tip is required to load the device with desired fluid. Automating a pipetting step in a scenario where the device is made out of a flexible material introduces technical complications. Passive pumping has been suggested as a viable alternative to contact pipetting[58]. In passive pipetting, a droplet of the liquid desired to be loaded into the device is dropped on the one of the inlets to the channel while the other larger inlet is also filled with a liquid meniscus (Figure 5.1 Passive pumping schematic). Due to differences in pressure at each inlet arising from surface tension, liquid is drawn into the channel in a controlled fashion. This technique could be used to dispense fluid into a device using an automated pipette without any contact.

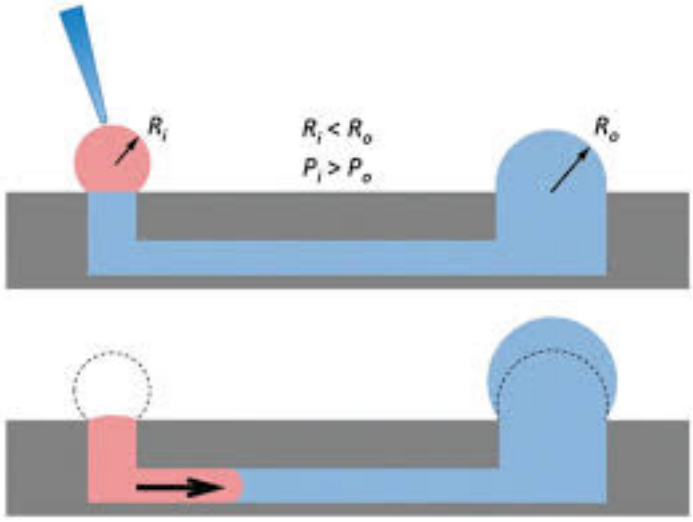

Figure 5.1 Passive pumping schematic

5.3.3 Device fabrication in Polystyrene

Hot embossing of microfluidic devices using polystyrene sheets[59] is a widely used method to produce hydrophilic devices at a lower cost than PDMS. Currently, since the devices are made out of PDMS, they need to be plasma activated and bonded just moments before their use.

Manufacturing devices out of polystyrene, would enable researchers to stock prefabricated and pre-coated devices and run experiments as biological samples are available. Precoating the device with the required ECM protein would also reduce the hands-on time required to run the experiment from 3 hours to 30 minutes.

Bibliography

1. Manahan, C. L., Iglesias, P. A., Long, Y. & Devreotes, P. N. CHEMOATTRACTANT SIGNALING IN *DICTYOSTELIUM DISCOIDEUM*. *Annu. Rev. Cell Dev. Biol.* **20**, 223–253 (2004).
2. Adler, J. Chemotaxis in Bacteria. *Science (80-.).* **153**, 708–716 (1966).
3. Dickinson, R. B. & Tranquillo, R. T. A stochastic model for adhesion-mediated cell random motility and haptotaxis. *J. Math. Biol.* **31**, 563–600 (1993).
4. Dusenberry, D. *Living at Micro Scale*. (Harvard University Press, 2011).
5. Smith, P. D. *et al.* Monocyte function in the acquired immune deficiency syndrome. Defective chemotaxis. *J. Clin. Invest.* **74**, 2121–8 (1984).
6. de Oliveira, S., Rosowski, E. E. & Huttenlocher, A. Neutrophil migration in infection and wound repair: going forward in reverse. *Nat. Rev. Immunol.* **16**, 378–391 (2016).
7. Phillipson, M. & Kubes, P. The neutrophil in vascular inflammation. *Nat. Med.* **17**, 1381–1390 (2011).
8. Dormann, D. & Weijer, C. J. Chemotactic cell movement during development. *Curr. Opin. Genet. Dev.* **13**, 358–364 (2003).
9. Roussos, E. T., Condeelis, J. S. & Patsialou, A. Chemotaxis in cancer. *Nat. Rev. Cancer* **11**, 573–87 (2011).
10. Zonneveld, R., Molema, G. & Plötz, F. B. Analyzing Neutrophil Morphology, Mechanics, and Motility in Sepsis: Options and Challenges for Novel Bedside Technologies. *Crit. Care Med.* **44**, 1–11 (2015).
11. Sackmann, E. K.-H. *et al.* Characterizing asthma from a drop of blood using neutrophil chemotaxis. *Proc. Natl. Acad. Sci. U. S. A.* **111**, 5813–8 (2014).
12. Butler, K. L. *et al.* Burn injury reduces neutrophil directional migration speed in microfluidic devices. *PLoS One* **5**, (2010).
13. Berthier, E., Surfus, J., Verbsky, J., Huttenlocher, A. & Beebe, D. An arrayed high-content chemotaxis assay for patient diagnosis. *Integr. Biol. (Camb).* **2**, 630–638 (2010).
14. Cicchetti, G., Allen, P. G. & Glogauer, M. C hemotactic S ignaling P athways in N eutrophils: from R eceptor to A ctin A ssembly. *Crit. Rev. Oral Biol. Med.* **13**, 220–228 (2002).
15. Tan, R. Z. & Chiam, K.-H. A computational model for how cells choose temporal or spatial sensing during chemotaxis. *PLOS Comput. Biol.* **14**, e1005966 (2018).
16. Heit, B., Colarusso, P. & Kubes, P. Fundamentally different roles for LFA-1, Mac-1 and alpha4-integrin in neutrophil chemotaxis. *J. Cell Sci.* **118**, 5205–20 (2005).
17. Wenceslau, C. F. *et al.* Mitochondrial-derived N-formyl peptides: Novel links between trauma, vascular collapse and sepsis. *Med. Hypotheses* **81**, 532–535 (2013).
18. Gambardella, L. & Vermeren, S. Molecular players in neutrophil chemotaxis-focus on PI3K and small GTPases. *J. Leukoc. Biol.* **94**, 603–612 (2013).
19. Everitt, E. A., Malik, A. B. & Hendey, B. Fibronectin enhances the migration rate of human neutrophils in vitro. *J. Leukoc. Biol.* **60**, 199–206 (1996).
20. Summers, C. *et al.* Neutrophil kinetics in health and disease. *Trends Immunol.* **31**, 318–24 (2010).
21. Irimia, D. Microfluidic Technologies for Temporal Perturbations of Chemotaxis. *Annu. Rev. Biomed. Eng.* **12**, 259–284 (2010).

22. Boyden, S. The chemotactic effect of mixtures of antibody and antigen on polymorphonuclear leucocytes. *J. Exp. Med.* **115**, 453 (1962).
23. Zigmond, S. H. Ability of polymorphonuclear leukocytes to orient in gradients of chemotactic factors. *J. Cell Biol.* **75**, 606–16 (1977).
24. Zicha, D., Dunn, G. A. & Brown, A. F. A new direct-viewing chemotaxis chamber. *J. Cell Sci.* **99 (Pt 4)**, 769–75 (1991).
25. Weiner, O. D. *et al.* Spatial control of actin polymerization during neutrophil chemotaxis. *Nat. Cell Biol.* **1**, 75–81 (1999).
26. Altschuler, S. J. & Wu, L. F. Cellular Heterogeneity: Do Differences Make a Difference? *Cell* **141**, 559–563 (2010).
27. Heppner, G. Tumor heterogeneity. *Cancer Res* **44**, 2259–65 (1984).
28. Kim, P. *et al.* Soft Lithography for Microfluidics: a review. *Biochip* **2**, 1–11 (2008).
29. Nguyen, N.-T., Huang, X. & Chuan, T. K. MEMS-Micropumps: A Review. *J. Fluids Eng.* **124**, 384–392 (2002).
30. Kirby, B. *Micro- and Nanoscale Fluid Mechanics*. (Cambridge University Press, 2010).
31. Mäki, A.-J. *et al.* Modeling and Experimental Characterization of Pressure Drop in Gravity-Driven Microfluidic Systems. *J. Fluids Eng.* **137**, 021105 (2014).
32. Burger, R. *et al.* Centrifugal microfluidics for cell analysis. *Curr. Opin. Chem. Biol.* **16**, 409–414 (2012).
33. Gorkin, R. *et al.* Centrifugal microfluidics for biomedical applications. *Lab Chip* **10**, 1758 (2010).
34. Dertinger, S. K. W., Chiu, D. T., Noo Li Jeon & Whitesides, G. M. Generation of gradients having complex shapes using microfluidic networks. *Anal. Chem.* **73**, 1240–1246 (2001).
35. Poudineh, M. *et al.* Profiling Functional and Biochemical Phenotypes of Circulating Tumor Cells Using a Two-Dimensional Sorting Device. *Angew. Chemie - Int. Ed.* **56**, 163–168 (2017).
36. Jeon, N. L., Baskaran, H., Dertinger, S. K. W. & Whitesides, G. M. Neutrophil chemotaxis in linear and complex gradients of interleukin-8 formed in a microfabricated device. **20**, (2002).
37. Chen, Y.-C. *et al.* Single-cell Migration Chip for Chemotaxis-based Microfluidic Selection of Heterogeneous Cell Populations. *Sci. Rep.* **5**, 9980 (2015).
38. Yang, K. *et al.* A dual-docking microfluidic cell migration assay (D2-Chip) for testing neutrophil chemotaxis and the memory effect. *Integr. Biol. (United Kingdom)* **9**, 303–312 (2017).
39. Yang, K. *et al.* M kit : A Cell Migration Assay Based on Microfluidic Device and Smartphone. *Biosens. Bioelectron.* **99**, 259–267 (2017).
40. Boneschansker, L., Yan, J., Wong, E., Briscoe, D. M. & Irimia, D. Microfluidic platform for the quantitative analysis of leukocyte migration signatures. *Nat. Commun.* **5**, 4787 (2014).
41. Sackmann, E. K. *et al.* Microfluidic kit-on-a-lid: A versatile platform for neutrophil chemotaxis assays. *Blood* **120**, (2012).
42. Kubo, I., Furutani, S. & Matoba, K. Use of a novel microfluidic disk in the analysis of single-cell viability and the application to Jurkat cells. *J. Biosci. Bioeng.* **112**, 98–101 (2011).

43. Lee, D. & King, M. R. Microcontact printing of P-selectin increases the rate of neutrophil recruitment under shear flow. *Biotechnol. Prog.* **24**, 1052–1059 (2008).
44. Vidula, M., Du, Y., Shim, J., Lo, E. & Khademhosseini, A. Generating spatially and temporally controllable long-range concentration gradients in a microfluidic device. *Bioeng. Proc. Northeast Conf.* **9**, (2009).
45. Zipursky, A., Bow, E., Seshadri, R. S. & Brown, E. J. *Leukocyte Density and Volume in Normal Subjects and in Patients With Acute Lymphoblastic Leukemia*. *Blood* **48**,
46. Lee, S. H., Heinz, A. J., Choi, S.-E., Park, W. & Kwon, S. Polymer based chemical delivery to multichannel capillary patterned cells. *Lab Chip* **11**, 605–8 (2011).
47. Amsden, B. Solute Diffusion within Hydrogels. Mechanisms and Models. *Macromolecules* **31**, 8382–8395 (1998).
48. Tinevez, J.-Y. *et al.* TrackMate: An open and extensible platform for single-particle tracking. *Methods* **115**, 80–90 (2017).
49. Scott, R. A. & Peppas, N. A. Highly crosslinked, PEG-containing copolymers for sustained solute delivery. *Biomaterials* **20**, 1371–1380 (1999).
50. Shin, M. K., Kim, S. K. & Jung, H. Integration of intra- and extravasation in one cell-based microfluidic chip for the study of cancer metastasis. *Lab Chip* **11**, 3880 (2011).
51. Koh, W. G., Itle, L. J. & Pishko, M. V. Molding of Hydrogel Microstructures to Create Multiphenotype Cell Microarrays. *Anal. Chem.* **75**, 5783–5789 (2003).
52. Maheshwari, G. & Lauffenburger, D. A. Deconstructing (and reconstructing) cell migration. *Microsc. Res. Tech.* **43**, 358–368 (1998).
53. Wu, J., Kumar-Kanojia, A., Hombach-Klonisch, S., Klonisch, T. & Lin, F. A radial microfluidic platform for higher throughput chemotaxis studies with individual gradient control. *Lab Chip* **18**, 3855–3864 (2018).
54. Berthier, E., Warrick, J., Yu, H. & Beebe, D. J. Managing evaporation for more robust microscale assays : Part 1. Volume loss in high throughput assays. *Lab Chip* **8**, 852 (2008).
55. Berthier, E., Warrick, J. & Beebe, D. J. Managing evaporation for more robust microscale assays Part 2 .† Characterization of convection and diffusion for cell biology ‡. 860–864 (2008). doi:10.1039/b717423c
56. Steeg, P. S. Tumor metastasis: mechanistic insights and clinical challenges. *Nat. Med.* **12**, 895–904 (2006).
57. Walker, G. M. *et al.* Effects of flow and diffusion on chemotaxis studies in a microfabricated gradient generator. *Lab Chip* **5**, 611–8 (2005).
58. Rosoff, W. J., McAllister, R., Esrick, M. A., Goodhill, G. J. & Urbach, J. S. Generating controlled molecular gradients in 3D gels. *Biotechnol. Bioeng.* **91**, 754–759 (2005).
59. Young, E. W. K. *et al.* Rapid prototyping of arrayed microfluidic systems in polystyrene for cell-based assays. *Anal. Chem.* **83**, 1408–1417 (2011).

Appendices

Appendix A

A.1 Simulation of gradient generation- Hydrogels

To understand the nature of the gradient created in the liquid phase through controlled release from a hydrogel, finite element modelling was done using COMSOL Multiphysics. Briefly, the microchannel was divided into two equal entities, each having a cuboid-like geometry (Figure 5.1). The bottom half was designated as the hydrogel, with a corresponding lower diffusion constant ($D = 2.8x10^{-13}$ m^2/s, obtained experimentally (Appendix C)) for fMLP. The top half constituted of the cell media, with a higher diffusion constant to fMLP ($D = 4.5x10^{-10}$ m^2/s) and zero starting concentration. A time dependant study was carried out for a simulated time of 120 minutes and the concentration profiles at various heights (within hydrogel, below interface, above interface). These results are presented in Figure 5.2. Each plot shows the concentration curves at various time points from the beginning of diffusion up to 2 hours.

The PEGDA bulk concentration curve shows the concentration profile in the center of the Hydrogel layer. As expected, the concentration profile frozen in the hydrogel at polymerization is still retained after 2 hours due to the low diffusion constant within the medium. Above the interface, within the liquid medium, it can be observed that a linear concentration gradient is generated, validating that the hypothesis that “gradient forcing” by the hydrogel could generate a gradient in the liquid.

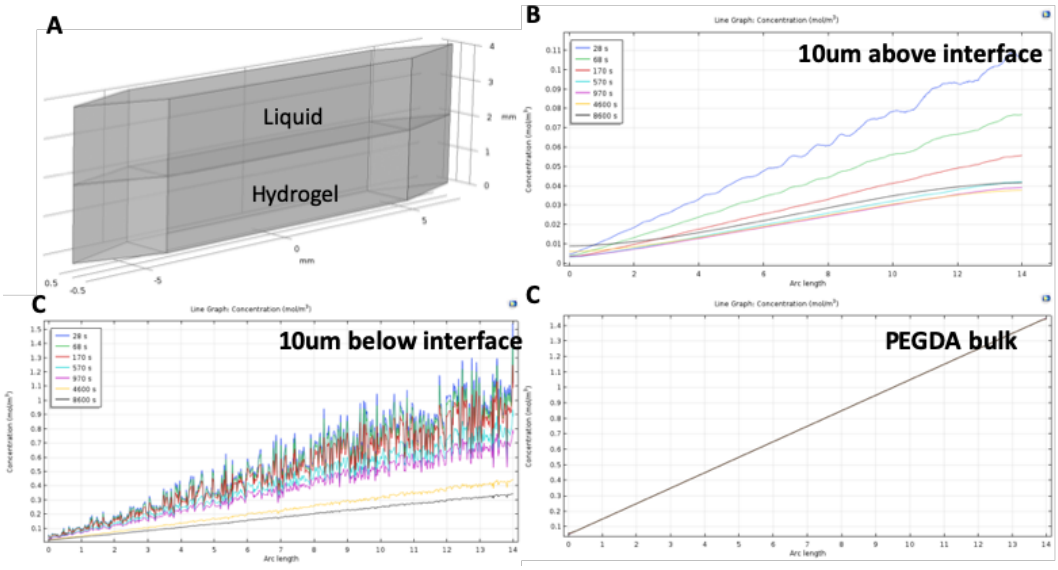

Figure 5.1 Simulation of linear gradient generation in a microfluidic channel using hydrogels

However, it is important to note the decreased strength of the gradient in the liquid as compared to the Hydrogel. The gradient strength is about 30 times lower in the liquid as compared to the gradient that was polymerized into the PEGDA. Analyzing the concentration profile below the interface in the PEGDA provides some clues to explain this observation. It can be noted that the gradient strength at the interface, while initially the same as the bulk, constantly decreases in magnitude due to the chemical molecules diffusing into the liquid medium. Owing to the low diffusion constant of the molecules inside PEGDA, this interface region is not replenished from the bulk. This effect can be observed in better detail in Figure 5.2, which shows a cross section of the interface. In the region spanning 100um above the interface, the concentration is almost close to 0 (a.u), while the corresponding region below the interface illustrates a gradient in concentration indicating the amount of leaching occurring in the hydrogel.

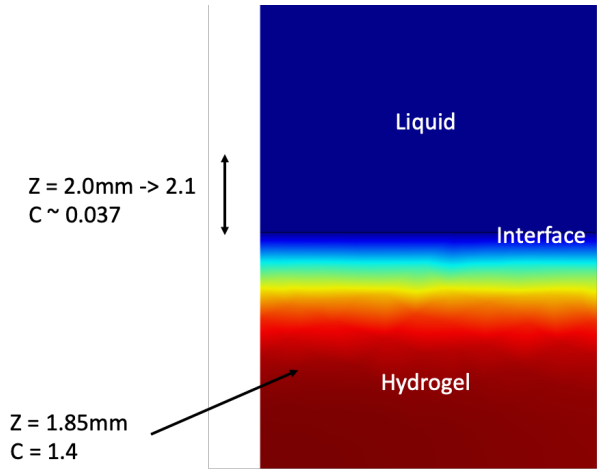

Figure 5.2 Chemical leaching within PEGDA at the liquid interface

A.2 Mould fabrication

The following rapid prototyping methods to fabricate moulds in negative were tested and prototyped. They can be broadly classified into additive and subtractive digital fabrication methods depending on whether material is progressively deposited or removed to achieve the desired end result. The following methods were chosen for their high fabrication resolution as well as ready access to the tools, making rapid design iteration cycles possible.

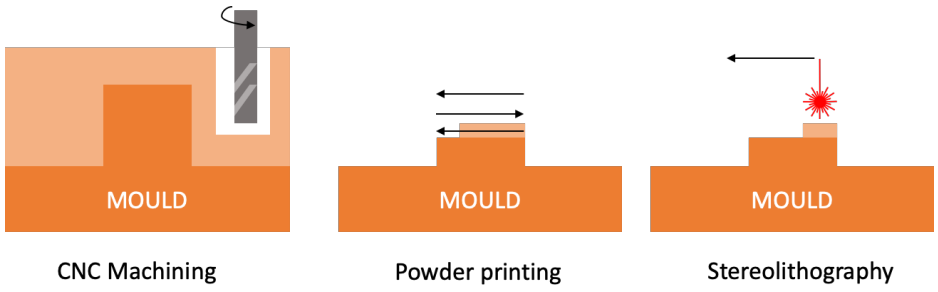

Figure 5.3 Overview of various rapid prototyping mould fabrication methods

Computer Numerical Control (CNC) routing is a controlled process of material removal using a rapidly rotating routing bit. As showing in Figure X, material can be gradually removed from

material stock to create a desired mould profile. The fabrication method imposes a few constraints on the features than can be achieved using this technique. The tool positioning resolution of the machine (Roland MDX-40), though important, is not the resolution limiting factor of the process given the choice of the material. The mould was chosen to be fabricated in modelling wax, due to system constraints as well as superior surface finish compared to other materials. The smallest feature that could be fabricated therefore depended on the strength of the residual material withstanding forces from the routing bit that could cause the feature to snap or break off the base. While the XY resolution at aspect ratios higher than 1 was limited to 200um, flatter features (<200um) could be fabricated at a 25um resolution. The diameter of the drilling bit (up to 1000um) placed an additional constraint on the minimum separation distance between two features in the mould. The number of flutes in the routing bit as well as its general quality influenced the final surface roughness of the device.

Extensive testing demonstrated the viability of this technique to create master negative moulds capable of creating PDMS devices. The sharpness of the resulting edges in the PDMS devices is to be noted, especially in comparison to the other techniques. The glass transition temperature of the modelling wax implied a room temperature curing process for PDMS, resulting in an overnight process. The disqualifying feature of this method however was the resulting surface roughness, which was unacceptable for chemotaxis assays. Cells were found to follow and move along the residual circular track resulting from the routing bit. As seen in the figure, the cell path over 5 minutes tracked in blue shows aberrations coinciding with the edges from the milling process. This can be contrasted with the hydrogel surface molded from a PDMS surface cast from a fluoropolymer sheet which is visibly smoother.

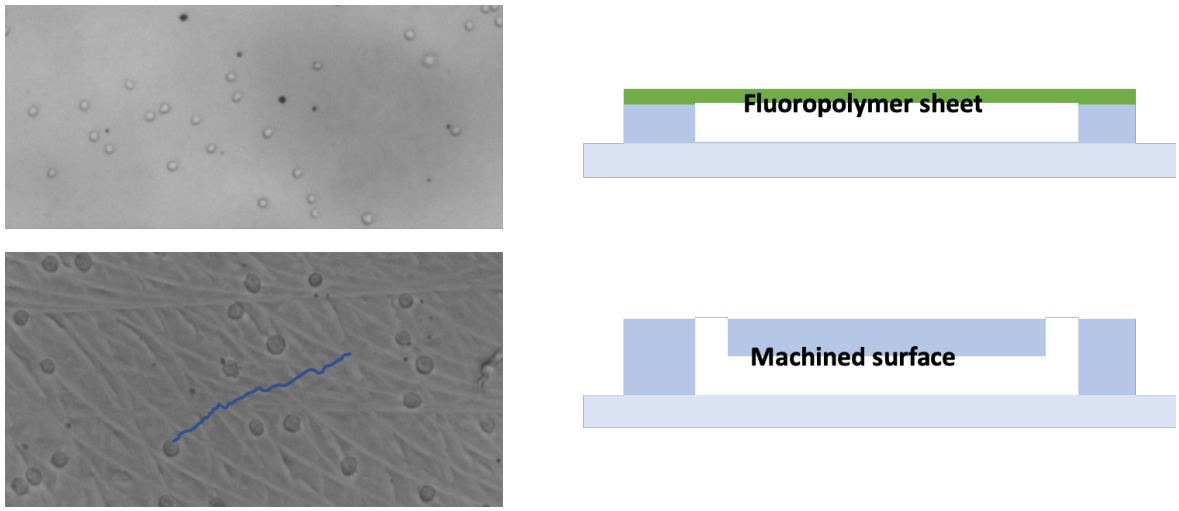

Figure 5.4 Surface roughness of hydrogels cast from CNC machined moulds

Powder printing is an additive 3D printing method, where the source material is progressively deposited as a power and UV cured to fuse the composite layer by layer into a solid final product. The Stratasys Objet 30Pro printer was used to make negative moulds both in VeroWhite and VeroBlue materials. The printed objects had an XY resolution of 100um and a Z resolution of 25um. However, the material was found to inhibit PDMS curing at the interface. To resolve this limitation, the printed material had to be subject to multi-day heat treatment process. This resulted in extensive reflow as documented in Figure X. As a result, achieving sharp edges and features of a controlled dimension were almost impossible.

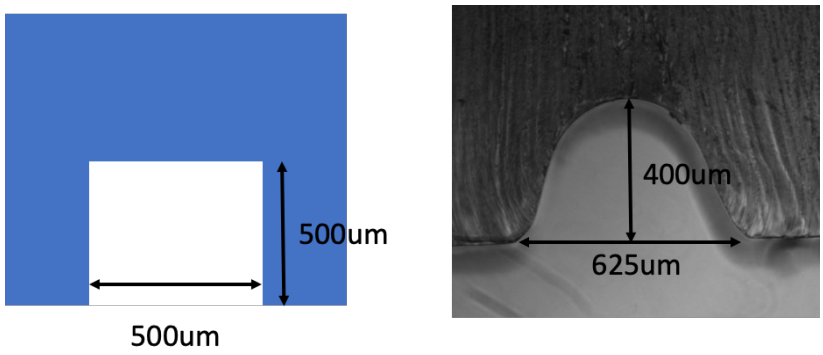

Figure 5.5 Heat reflow of powder printed mould at 65 degrees Celsius after 1 hour.

Commercial Stereolithography is an additive manufacturing process wherein material is photopolymerized using a UV laser focused to a point. Using Galvo mirrors, the location of the laser spot is moved around in a controlled fashion to achieve the desired shape in a layer by layer fashion. The moulds used in this thesis were fabricated in Somos WaterShed XC11122 material by Protolabs, Inc. USA. The resulting moulds had a X, Y resolution of 50um and a Z resolution of under 25um. Additionally, the mould was heat stable resulting in well-defined channel edges. Commercial stereolithography was therefore the method of choice for the PDMS mould for most subsequent device designs.

A.3 Fabrication of through cut PDMS layers

Traditional PDMS fabrication processes manually punch inlet holes, which is not feasible in high throughput devices due to the sheer number as was as the variability introduced. Therefore, there is a need to fabricate inlet holes through the soft lithography moulding process as well. Additionally, there is a need to fabricate through-cut PDMS sheets for the hydrogel molding process.

Various groups have proposed methods to achieved through-cut PDMS, of which foremost is the use of a fluoropolymer sheet (3M Scotchpak 9744) to press down on the PDMS filled mould to squeeze out all the material between the mould feature corresponding to the inlets and the sheet. Once cured in this state, the PDMS device can be extricated from the mould along with the sheet that is now capable of acting as a backing layer for extremely thin PDMS layers as well. This assembly can be irreversibly plasma bonded to glass, after which the fluoropolymer sheet can the peeled off due to the higher bond strength of the PDMS to glass. The resulting device does not require any manual hole punching and is therefore suitable for larger scale device assembly in a context where repeatability is important.

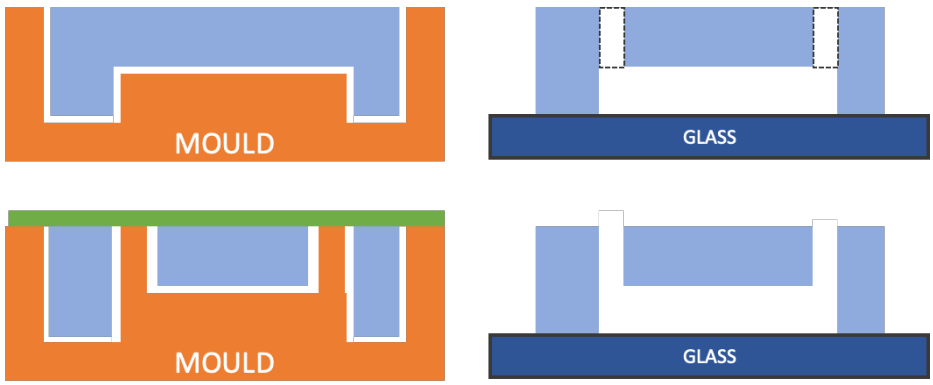

Figure 5.6 Through-cut PDMS layer fabrication (fluoropolymer sheet in green)

Appendix B Multilayer PDMS fabrication

Multilayered PDMS devices are usually fabricated by stacking multiple two-dimensional layers to greatly increase the functionality of 2D microfluidic channels. Complex flow control

structures can be fabricated using multilayered devices. Multilayered devices can be designed to be modular, eliminating the need for off-chip tubing to connect various devices. Devices requiring overhanging structures, which cannot be released from a single mould can also be realized through multilayered devices.

However, multilayered devices pose unique fabrication challenges. PDMS is a flexible elastomer making the assembly and bonding of several sheets with precise alignment difficult. The low Young's modulus of PDMS renders traditional mechanical jigs impractical for alignment. The bonding of PDMS to PDMS and glass is usually accomplished through a process of plasma bonding which is irreversible due to formation of strong bonds. This provides for a single attempt at alignment by bringing the two plasma-activated surfaces into contact. A combination of the low Young's modulus as well as the provision of only a single attempt at bonding makes fabrication of multi-layer devices non-trivial. Various strategies that have been attempted at addressing multilayer PDMS alignment and bonding issues deal with one of these two issues, or both.

A thin film of methanol has been proposed as a means to lubricate the two plasma treated PDMS layers during the process of manual alignment. The presence of methanol prevents the immediate formation of bonds, while still stabilizing the silanol bonds created during the plasma oxidation process. The bonds therefore only form once the methanol is evaporated. Methanol lets the two layers slide freely with respect to each other, eliminating any stress in/between layers that can lead to strain and improper registration of alignment features.

Isotropic shrinkage of up to 1 percent by length occurs during the elevated-temperature curing process of PDMS (usually at 65 degrees Centigrade). While this shrinkage is not significant for devices as large as a few millimeters (shrinkage is a few tens of micrometers), it is crucial to the design process in a wafer batch-process, where millimeter sized devices are distributed throughout a 2-inch (50mm) or a 4-inch (100mm) wafer. A few methods have been suggested to address the shrinkage issue. Some have suggested curing PDMS at a room temperature to minimize shrinkage, while others have proposed scaling the PDMS mould itself by a suitable factor to offset the shrinkage ratio.

B.1 Techniques for PDMS alignment

In the subsequent sections, the following methods for inter-layer PDMS alignment have been tested and characterized.

Manual alignment using spacers

PDMS layers were bonded to each other after plasma oxidation of both surfaces. A process of manual alignment by eye was used to align features on both layers to each other. To prevent irreversible bonding between surfaces during the process of alignment, spacers made out of cardstock material was used. After satisfactory alignment, the spacers were slid out from between the layers thereby bonding them permanently. Though simple, this method had numerous disadvantages. Plasma activated PDMS samples form strong bonds only when bonded under a certain time after activation. This placed an unreasonable constraint on the speed with

which manual alignment and bonding had to be done. Due to the high surface energy of PDMS surfaces, choosing a suitable spacer material that would not "catch" on the PDMS layers when pulled out was difficult. Smooth cardstock was the best material that was readily available, but nevertheless did not slide out perfectly. Thin PDMS layers also posed a problem, due to higher flexibility and capability to bond to the bottom layer through gaps in the spacer layer as compared to thicker sheets.

Jigs and Alignment Features

Alignment features such as rectangles were integrated into each layer and designed to be through cut as shown in Figure 3.11. 3D printed jigs were then designed to be press fit into the alignment features, enabling other layers to be stacked upon.

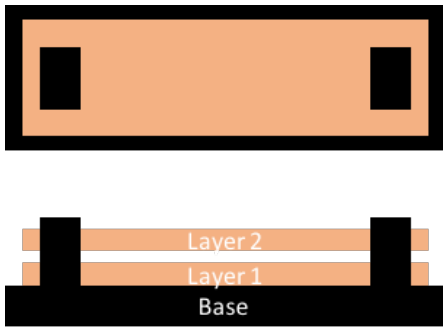

Figure 5.7 Multilayer PDMS alignment using a 3D printed jig

This alignment method also faced several challenges to successful implementation. The flexibility of PDMS, while enabling the Jigs to be press-fit into the features, does create

opportunities for PDMS to stretch and cause misalignment at locations on the device where an alignment feature is not close by. Thin layers posed a similar problem as observed with Manual alignment where the flexion in the layer cause unwanted bonding.

Wafer handles and Jigs

To bypass the issue of PDMS flexibility, each PDMS layer was cured along with a 3D printed handle. The mould for had features to fix the handle, and the PDMS was poured into mould after the handle was fixed. This whole assembly was later cured at room temperature. As an alternative to aligning flexible sheets of PDMS to each other, the comparatively inflexible handles were aligned to each other using a dowel pin jig. The entire process is demonstrated in this figure

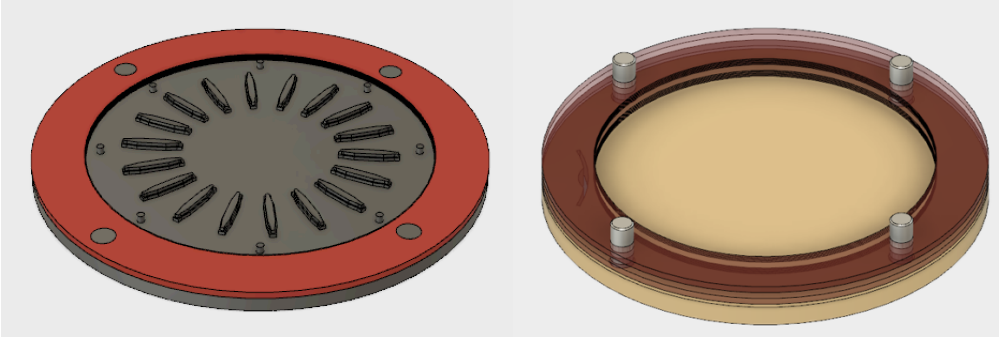

Figure 5.8 Casting flexible PDMS layers in rigid handles. These layers are aligned to each other through features in the rigid handles.

Methanol and Feature registration

In this alignment method, the problem of one-shot irreversible bonding that is usually observed with plasma activated PDMS surfaces is circumvented by using methanol as a lubricant as well as a medium to prolong the surface activation effect. After plasma oxidation of both the layers required to be bonded, methanol is immediately dispensed on one of the layers (the first layer). The second layer is then placed on top of the first layer creating a thin film of methanol separating the two layers and preventing immediate bonding. A jig is then used to align the 8 alignment holes on the circumference of each layer to each other as shown in the figure below.

After all the methanol has evaporated, the assembly is allowed to rest for an hour and the PDMS is then removed off the jig to be used.

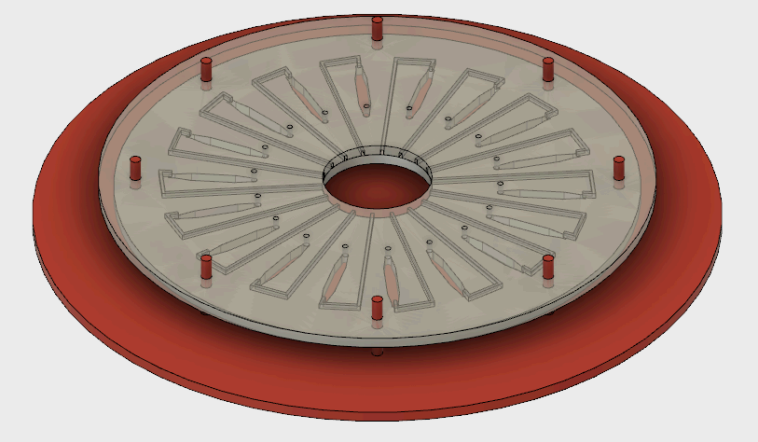

Figure 5.9 Multilayer Alignment of PDMS layers using through-cut alignment features

B.2 Characterization and Results

The efficacy of various alignment techniques was compared using an optical technique. PDMS devices after alignment were placed on a flat-bed scanner capable of recording images with a

resolution of 3000dpi. These scanned images were manually processed in ImageJ to quantify the absolute misalignment distance measured in micrometers for each single device on the wafer. An example of this workflow is shown below

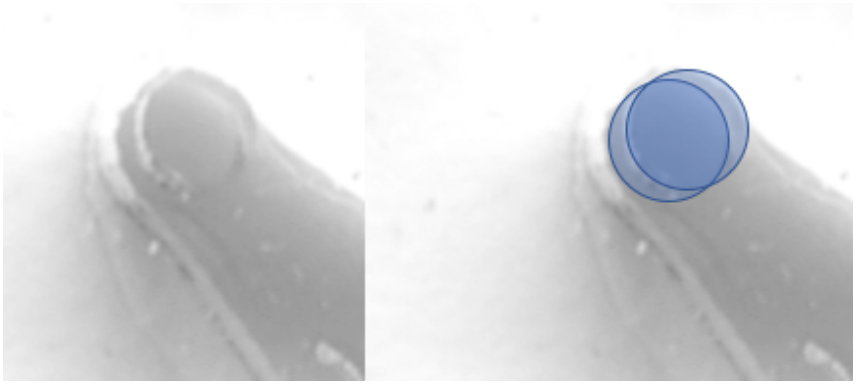

Figure 5.10 Quantification of misalignment as measured through visual microscopy

The misalignment was calculated for each device on the wafer and plotted as a Radar chart to schematically denote the misalignment across the wafer. Each curve on the chart represents one experiment

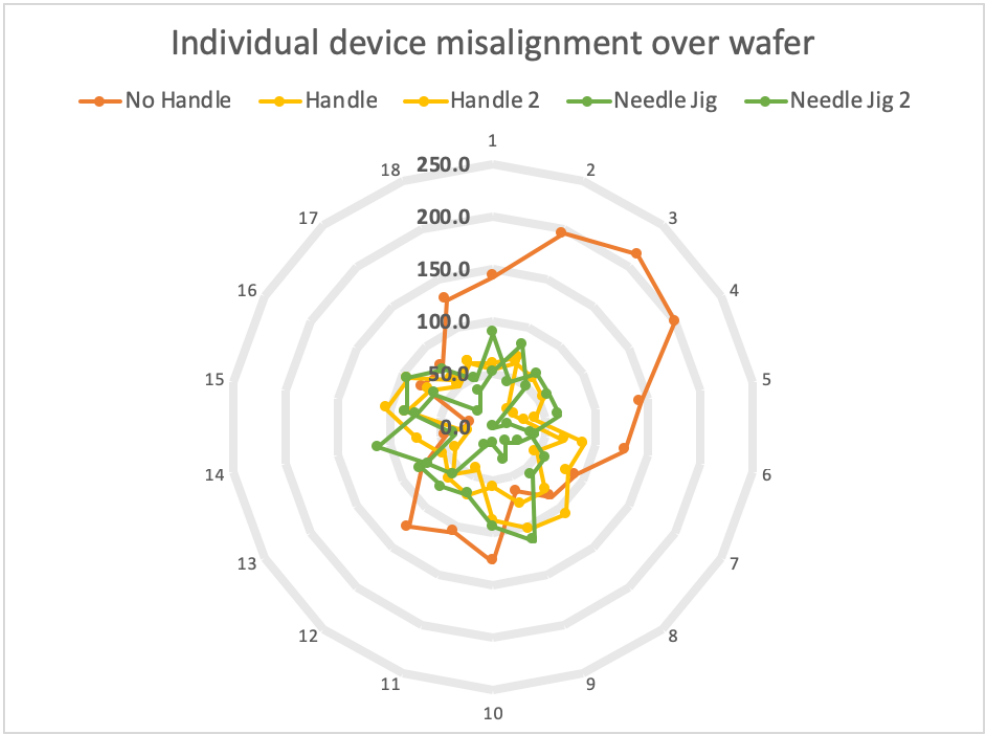

Figure 5.11 Wafer level device misalignment

The concentric circles denote a scale for the absolute misalignment, while the different positions along each curve circle show the misalignment at each of the 18 devices on a wafer scale. To put the numbers for the absolute misalignment into context, the features being aligned are 500um in diameter. The graph shows alignment under three different conditions

- Methanol without the use of a handle or a Jig - Labelled “No Handle”
- Use of a layer handle for alignment – Labelled “Handle”
- Use of Methanol and an alignment jig – Labelled “Needle Jig”

Clearly, the use of a method without a handle or jig resulted in poorer alignment, with some devices on the wafer being almost completely misaligned. The high variability demonstrates one of the major pitfalls of the manual alignment process for wafer-level alignment, the ability to locally align a single device but not over the entire wafer. The use of a handle for alignment as

well as methanol and a jig both yielded superior results, with average misalignment reduced from 140um to 65um. There was no statistically significant difference between either technique.

Appendix C Diffusion constant of chemoattractant (fMLP) in polymerized PEGDA 575

A 50% volume solution of PEGDA-575 in TE Buffer was the pre-polymer mix of choice to create a hydrogel with the desirable characteristics for gradient generation. The choice of hydrogel monomer as well as the volume ratios were established by previous unpublished work from the Multiscale Design lab. The diffusion coefficient therefore depends on various parameters relevant to the formation of the hydrogel such as the monomer and photo-initiator concentration as well as curing time. Experimentally, the diffusion constant can be estimated by quantifying the controlled release of the solute into the surrounding liquid from a geometrically well-defined hydrogel. The data from this experiment could either be fit against approximate analytical solution of the diffusion equation or numerical solution derived from finite element model (FEM) simulations. The diffusion constant thus obtained is used to simulate the gradient generation in liquid.

C.1 Materials and Methods:

PEGDA of molecular weight 575KDa was made up to a 50% by volume solution through dilution with TE Buffer. Irgacure 819 at 0.1% w/v was used as the photo initiator. 10mg of Rhodamine dye was added to 1ml of the solution. The solution was vortexed, incubated overnight at 37 degrees C and passed through a 0.22um syringe filter to remove undissolved photo initiator particles. The solution was used to fill a PDMS channel shaped like a disc and exposed to a custom 365nm UV light setup for 30 seconds to create the polymerized hydrogel. Cylindrical discs of controlled dimensions were thus formed with a 2.5mm radius and 0.625mm height. The discs were added to a flat-bottomed glass bottle with 5ml of DI water. 20μL of this solution was sampled periodically, whose concentration was estimated using a spectrophotometer. Serial dilution of Rhodamine was

also performed to obtain a calibration curve for concentration from spectrophotometry data. The data obtained was corrected to account for the sample volume removed.

C.2 Hydrogel simulations in COMSOL Multiphysics

COMSOL Multiphysics was used to perform time dependent FEM simulations of the diffusion phenomena using the "Transport of diluted species" physics library. The PEGDA disc was assumed to have a constant homogeneous diffusion coefficient 'D' for Rhodamine, and the value for the diffusion constant in water was obtained from work published by Gendron et al. The model and simulation were capable of measuring the average concentration of solute that was present in the surrounding solution at a given time. A parametric sweep of the expected Rhodamine diffusion constant 'D' was carried out to obtain the release kinetics.

Diffusion constant of rhodamine/fMLP in polymerized PEGDA the simulation results with a Rhodamine-in-PEGDA diffusion constant, 'D' of 2.8×10^{-13} m^2/s fit (minimize the R2 squared value among other options at a 0.1×10^{-13} m^2/s resolution) the experimental data of Rhodamine release from a PEGDA disk. As expected, a higher diffusion constant in the hydrogel led to faster release of chemical from the disk.

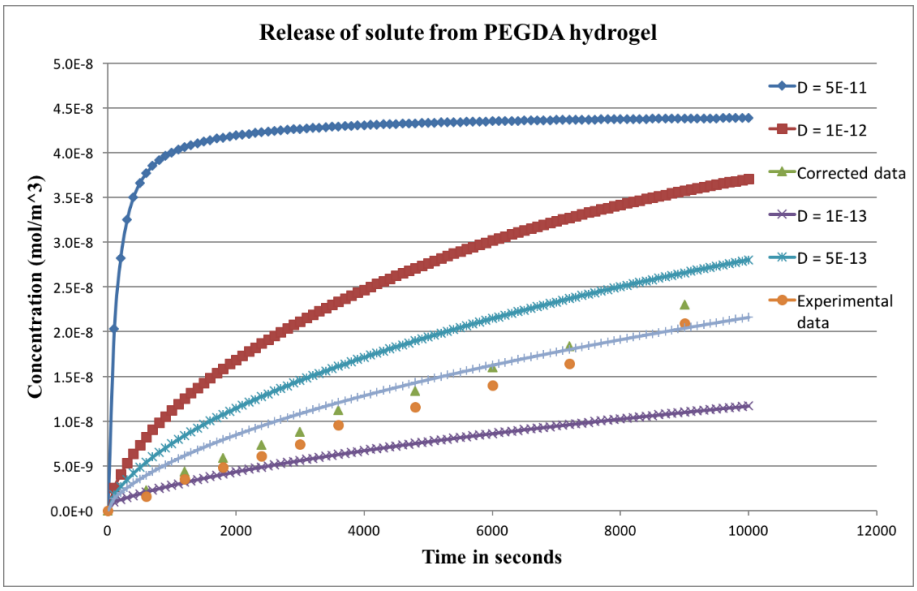

Figure 5.12 Fitting of simulation data with experimental results to extract diffusion constant for Rhodamine

Appendix D Materials and methods - Hydrogel chemotaxis device

In this section the finalized device fabrication and assembly, which were informed by the constraints and unique considerations outlined in the previous sections, will be presented. This protocol is used for all subsequent chemotaxis experiments with biological cells.

An overview of the device, showing its various components and assembly units to create the final device for running chemotaxis assays is shown in figure 3.16. The device is made up of 4 PDMS layers as well as a 2-inch glass wafer acting as the bottom surface for the assembly. The glass slide, along with layers 1 and 2 form the assembly required for hydrogel molding through polymerization. Subsequently, the cell loading assembly made up of layers 3 and 4 is aligned and placed on the exposed hydrogels. After cells are added into the device, the entire unit is placed on a spin coated for the alignment process following which time-lapse imaging is performed on a microscope with an automated stage.

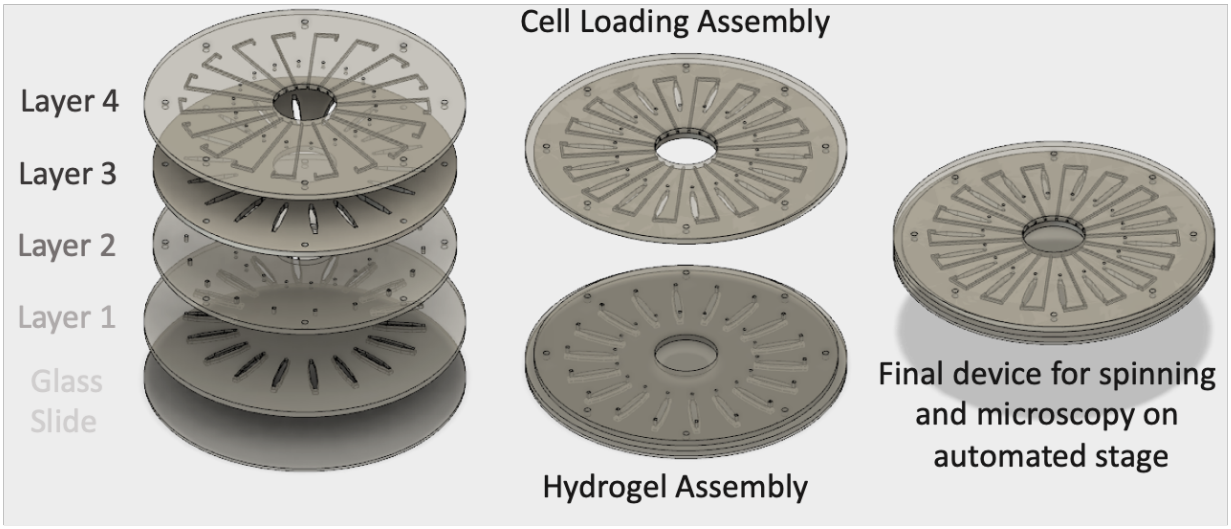

Figure 5.13 Overview of the hydrogel device assembly process

CNC machining was the mould fabrication method of choice. For alignment, the methanol technique was used for plasma bonding while a jig was used for reversible contact bonding as well as laser cut acrylic tape bonding. As a result each PDMS layer had 8 through-cut alignment features distributed across the area.

D.1 Fabrication of the PDMS layers

- The 4 PDMS layers were fabricated through the soft lithography process, combined with the through cut fabrication method described in section 3.4.2.
- Briefly, components A and B of Sylgard 184 (Dow Corning) was mixed in the ratio recommended by the manufacturer and degassed in a vacuum desiccator.
- The mixture was poured in the CNC machined moulds and further degassed
- The fluoropolymer sheet (3M Scotchpak 9722) was placed on the PDMS filled moulds, followed by a silicone sheet (40Duro, McMaster-Carr). 5kg of weight was placed on the sheet to expel the PDMS between the sheet and the through-cut features in the moulds
- The assembly was placed on a level surface for overnight curing at room temperature.

D.2 Hydrogel molding assembly

- Layer 1 was irreversibly bonded with a pre-cleaned glass wafer (University wafers) through plasma bonding (Harrick Plasma PDC-001). The plasma was created an a “High” intensity setting for 90 seconds at 750mTorr of pressure. Alignment was achieved by design as both the wafer as well as layer 1 were the same size.
- Layer 2 was reversibly bonded to Layer 1 by plasma activation of only one of the two surfaces. The methanol alignment technique with a custom needle jig was used for alignment.

D.3 Cell loading assembly

- Layer 3 was irreversibly bonded to Layer 4 by plasma activation of only one of the two surfaces. The methanol alignment technique with a needle jig was used for alignment
- A laser cut (VLS 2.30) acrylic tape (3M 4502) was bonded to the underside of Layer 3 with the backing layer attached. The acrylic tape was cut with the outlines of the main channels as well as the alignment features.

D.4 Chemical Materials and Methods

- A 50% PEGDA prepolymer solution was made up by mixing PEGDA 575 (Sigma Aldrich), TE Buffer (pH 8.0, Sigma Aldrich) and Ethyl Alcohol (Sigma Aldrich) in a 50:45:5 ratio. A Irgacure 2959 (Ciba-Geigy) in powder form was added to make up a final solution at a concentration 0.1 mg/ml. This solution was incubated at 37c overnight for dissolution followed by syringe filtering through a 0.33um filter for removal of large undissolved particles. The solution was stored in an opaque tube at room temperature for up to 2 weeks.
- Lyophilized fMLP (Sigma Aldrich) was dissolved in DMSO to make up a 10mM stock solution of the chemoattractant stored at -20c for up to a month. Aliquots were thawed and diluted in TE buffer, and subsequently mixed into prepolymer solutions. These solutions were stored at 4c for up to a week.

D.5 Biological materials and methods

- Human Leukemia cell line (HL60) was obtained from ATCC and maintained in RPMI-1640 medium supplemented by 1% Antibiotic/Antimycotic and 10% Heat inactivated Fetal Bovine Serum. Cells were cultured twice a week.

- Differentiation into neutrophil like cells (dHL-60) was done by addition of 1.3% DMSO according to standard procedures. Cells were used for chemotaxis experiments 5 to 7 days after differentiation.
- On the day of the experiment, differentiated HL60 cells was twice washed in RPMI-1640 to remove FBS and replace the culture medium with the migration medium.

D.6 Chemotaxis assay

- 15 microliters (uL) of PEGDA media was pipetted into the channel, followed by 15 µL of PEGDA with fMLP/Rhodamine
- After waiting for 5 minutes for the gradient in the liquid pre-polymer to diffuse, the device was placed on top of a 365nm UV curing machine at a distance for 5cm for 1.2 seconds to fully polymerize the hydrogel.
- Immediately after polymerization, the layer containing the square inlet holes was removed and the cell loading assembly aligned with the channels containing the hydrogel.
- 30 µL dHL60 cells in the cell migration medium was added to each device
- The assembly was placed on a spin coater chuck that automatically centred the substrate. The device was then spun @ 2000 rpm for 60 seconds with an acceleration and deceleration cycles of 100rpm/min
- Devices were subsequently moved to a humidified chamber on the automated stage top of a microscope, where time lapse imaging was performed at the barrier feature to capture images every 15 seconds for 1 hour.

D.7 Image processing and analysis

- The TrackMate plugin in imageJ was used to process the timelapse recordings to obtain cell tracks. This plugin is intuitive to use and capable of cell segmentation as well as tracking.
- Briefly, a rectangular area of the image that is desired to be analyzed is specified as well as the expected particle diameter for cell segmentation.
- Various parameters such as quality, standard deviation etc. can be used to remove blobs resulting from background noise and debris.
- After filtering to achieve satisfactory segmentation, the tracking algorithm is run to compare the position of the blobs from one frame to the next, linking closest neighbours. This analysis limitation places a constraint on the density of cells.
- Once cell tracks are analyzed, the results can be saved in an XML format. These results were analyzed using a custom python script that is capable of parsing the XML file and generating key output metrics such as net migration distance, velocity, chemotactic index and persistence.